

Energies of B_s meson excited states — a lattice study

(UKQCD Collaboration)

J. Koponen^{1,*}

¹*Department of Physics and Helsinki Institute of Physics,
P.O. Box 64, FIN-00014 University of Helsinki, Finland*

(Dated: September 10, 2021)

Abstract

This is a follow-up to our earlier work on the energies and radial distributions of heavy-light mesons. The heavy quark is taken to be static (infinitely heavy) and the light quark has a mass about that of the strange quark. We now concentrate on the energies of the excited states with higher angular momentum and with a radial node. A new improvement is the use of hypercubic blocking in the time direction.

The calculation is carried out with dynamical fermions on a $16^3 \times 32$ lattice with a lattice spacing $a \approx 0.1$ fm generated using a non-perturbatively improved clover action.

In nature the closest equivalent of this heavy-light system is the B_s meson, which allows us to compare our lattice calculations to experimental results (where available) or to give a prediction where the excited states, particularly P-wave states, should lie. We pay special attention to the spin-orbit splitting, to see which one of the states (for a given angular momentum L) has the lower energy. An attempt is made to understand these results in terms of the Dirac equation.

*Electronic address: jonna.koponen@helsinki.fi

I. MOTIVATION

There are several advantages in studying a heavy-light system on a lattice. First of all, the lattice calculations are relatively easy to do, and it allows us to do these with QCD from first principles. Our meson is much more simple than in true QCD: one of the quarks is static (infinitely heavy) with the light quark “orbiting” it. This makes it very beneficial for modelling. On the lattice an abundance of data can be produced, and we know which state we are measuring. In contrast, the physical states can be a mixture of two or more configurations, but on the lattice this complication is, mostly, avoided. Even so, our results on the heavy-light system can still be compared to the B_s meson experimental results.

II. MEASUREMENTS AND LATTICE PARAMETERS

We measure the energies of both angular and first radial excitations of heavy-light mesons. Since the heavy quark spin decouples from any description of the configurations we may label the states as $L_{\pm} = L \pm \frac{1}{2}$, where L is the orbital angular momentum and $\pm\frac{1}{2}$ refers to the spin of the light quark.

The measurements are done on $16^3 \times 32$ lattices using two degenerate quark flavours. The lattice configurations were generated by the UKQCD Collaboration using lattice action parameters $\beta = 5.2$, $c_{\text{SW}} = 2.0171$ and three different values for the hopping parameter κ (see Table I). The three different lattices are referred to here as “DF3”, “DF4” and “DF5”. Each of them has a slightly different lattice spacing (a) and a different light quark mass (m_q). Our main results are measured on the “DF3” lattice, because the light quark mass is very close to the strange quark mass. More details of the lattice configurations used in this study can be found in Refs. [1, 2]. Because our light quarks are heavier than true u and d quarks, we have m_{π} ranging from 730 MeV (“DF3”) to 400 MeV (“DF5”). Two different levels of fuzzing (2 and 8 iterations of conventional fuzzing) are used in the spatial directions to permit a cleaner extraction of the excited states.

III. 2-POINT CORRELATION FUNCTION

The 2-point correlation function (see Fig. 1) is defined as

$$C_2(T) = \langle P_t \Gamma G_q(\mathbf{x}, t+T, t) P_{t+T} \Gamma^\dagger U^Q(\mathbf{x}, t, t+T) \rangle, \quad (1)$$

where $U^Q(\mathbf{x}, t, t+T)$ is the heavy (infinite mass)-quark propagator and $G_q(\mathbf{x}, t+T, t)$ the light anti-quark propagator. P_t is a linear combination of products of gauge links at time t along paths P and Γ defines the spin structure of the operator. The $\langle \dots \rangle$ means the average over the whole lattice. A detailed discussion of lattice operators for orbitally excited mesons can be found in [3]. In this study, the same operators are used as in [4]. The energies (m_i) and amplitudes (a_i) are extracted by fitting the C_2 with a sum of exponentials,

$$[C_2(T)]_{f_1, f_2} \approx \sum_{i=1}^{N_{\max}} a_{i, f_1} e^{-m_i T} a_{i, f_2}, \text{ where } N_{\max} = 2 - 4, T \leq 14. \quad (2)$$

The fit is a simple least squares fit. In most of the cases 3 exponentials are used to try to ensure the first radially excited states are not polluted by higher states. Also 2 and 4 exponential fits are used to cross-check the results wherever possible. Indices f_1 and f_2 denote the amount of fuzzing used at the vertices and both of them take two values, $f_1 = \text{F1, F2}$ and $f_2 = \text{F1, F2}$, where (F1=2 iterations and F2=2+6 iterations). For S and P₋ states we have alternative operators (see [4]), so we get a 5 by 5 matrix (5 paths, because one operator has two choices, F1 and F2, and the other operator has three choices, local, F1 and F2) instead of just a 2 by 2 matrix (2 paths) given by the fuzzing choices.

	κ	r_0/a	a [fm] (approx.)	m_q/m_s (approx.)	$r_0 m_\pi$	No. of configs.
DF3	0.1350	$4.754(40)_{-90}^{+2}$	0.110	1.1	1.93(3)	160
DF4	0.1355	$5.041(40)_{-10}^{+0}$	0.104	0.6	1.48(3)	119
DF5	0.1358	5.32(5)	0.099	0.3	1.06(3)	139

TABLE I: Lattice parameters (from [1]). The Sommer scale parameter can be taken to be $r_0 = 0.525(25)$ fm and m_s is the s quark mass.

IV. SMEARED HEAVY QUARK

We introduce two types of smearing in the time direction to get a better noise to signal ratio. The first type is APE type smearing, where the original links in the time direction are replaced by a sum over the six staples that extend one lattice spacing in the spatial directions (in Fig. 2 on the left). This smearing is called here “sum6” for short. We use the notation “plain” to refer to the original Eichten–Hill point static source construction.

To smear the heavy quark even more we then use hypercubic blocking (first introduced by Hasenfratz and Knechtli in [5]), again only for the links in the time direction (in Fig. 2 on the right). Now the staples (the red dashed lines in Fig. 2) are not constructed from the original, single links, but from staples (the blue dash-dotted lines in Fig. 2). In more detail, we first construct the links

$$\bar{V}_{i,\mu;\nu\rho} = \text{Proj}_{\text{SU}(3)} \left[(1 - \alpha_3) U_{i,\mu} + \frac{\alpha_3}{2} \sum_{\pm\eta \neq \rho, \nu, \mu} U_{i,\eta} U_{i+\hat{\eta},\mu} U_{i+\hat{\mu},\eta}^\dagger \right], \quad (3)$$

where $U_{i,\mu}$ is the original thin link at location i and direction μ . Note that there are no staples in directions ν or ρ . We then construct “fat” links

$$\tilde{V}_{i,\mu;\nu} = \text{Proj}_{\text{SU}(3)} \left[(1 - \alpha_2) U_{i,\mu} + \frac{\alpha_2}{4} \sum_{\pm\rho \neq \nu, \mu} \bar{V}_{i,\rho;\nu\mu} \bar{V}_{i+\hat{\rho},\mu;\rho\nu} \bar{V}_{i+\hat{\mu},\rho;\nu\mu}^\dagger \right], \quad (4)$$

where index ν indicates that the link is not decorated with staples in that direction. The last step is

$$V_{i,\mu} = \text{Proj}_{\text{SU}(3)} \left[(1 - \alpha_1) U_{i,\mu} + \frac{\alpha_1}{6} \sum_{\pm\nu \neq \mu} \tilde{V}_{i,\nu;\mu} \tilde{V}_{i+\hat{\nu},\mu;\nu} \tilde{V}_{i+\hat{\mu},\nu;\mu}^\dagger \right], \quad (5)$$

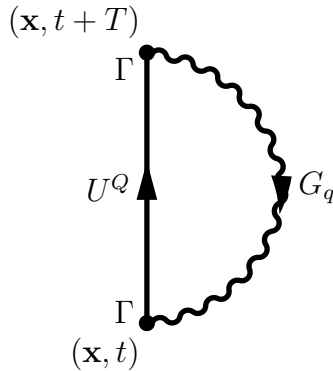


FIG. 1: Two-point correlation function.

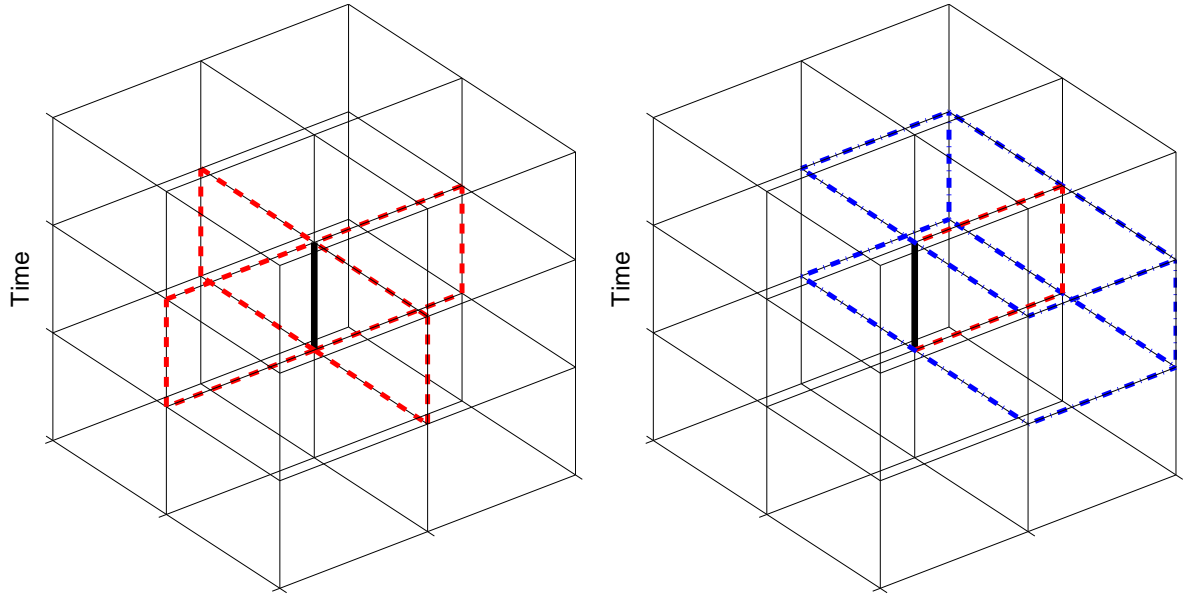


FIG. 2: (Color online) APE smearing in the time direction (on the left) and hypercubic blocking (on the right).

where the “fat” links are again used to construct the new links. The values $\alpha_3 = 0.5$, $\alpha_2 = 1$ and $\alpha_1 = 1$ are used in this study, because this choice was found to be very good in reducing the noise to signal ratio in [6]. Note that $\alpha_3 = 1.0$, $\alpha_2 = 0$ and $\alpha_1 = 0$ would give the “sum6” smearing. Hypercubic blocking takes into account the links within a “hypercube” (the edges of the “cube” are $2a$ in spatial directions but only one lattice spacing in the time direction). This smearing is called here “hyp” for short. The “plain” configurations do not have smearing in the time direction. Smearing the heavy quark improves the noise to signal ratio, which can be seen in Figs. 3–7. The figures show the standard deviation to signal ratio for the largest component of C_2 , which is F2F2, for 160 lattice configurations (lattice “DF3”). In all cases the “plain” signal is clearly inferior to the “sum6” and “hyp” signals, whereas the “hyp” signal is also better than the “sum6” signal. This latter difference would be more apparent in a non-logarithmic scale. Lattices “DF4” and “DF5” show similar trends as the “DF3” lattice.

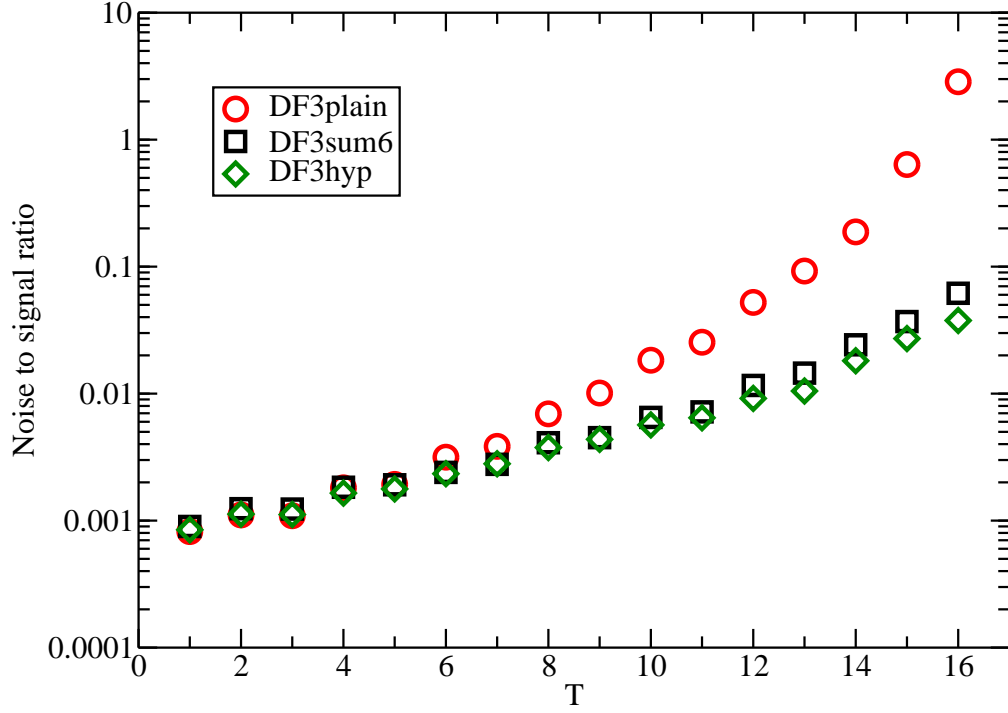


FIG. 3: (Color online) Noise (standard deviation) to signal ratio: S-wave 2-point correlation function C_2 for the lattice “DF3”. Note the logarithmic scale.

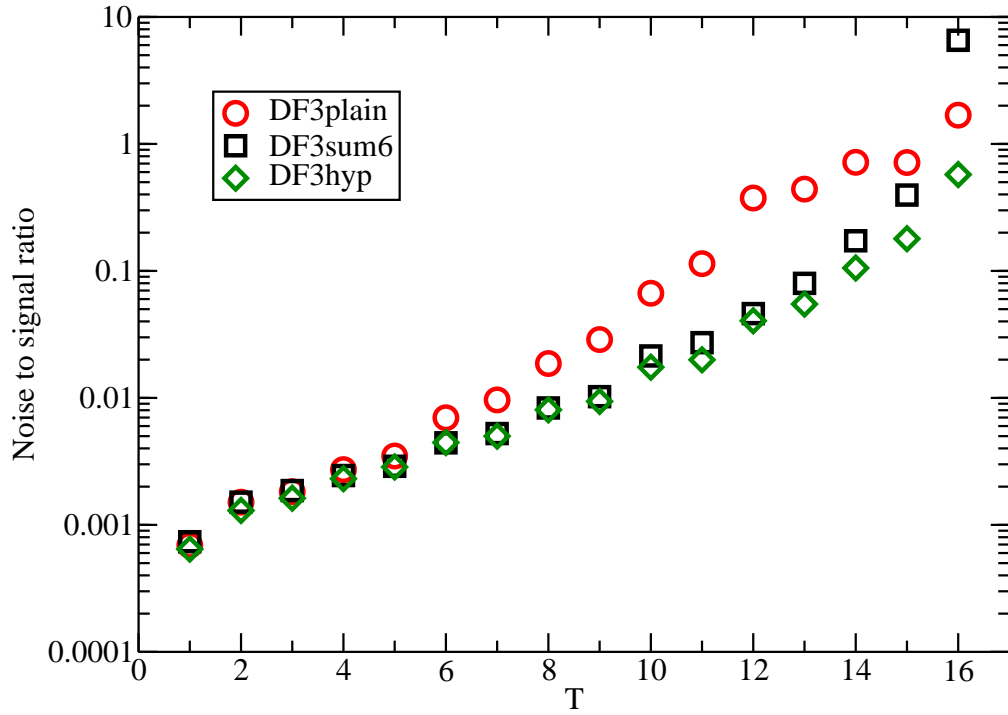


FIG. 4: (Color online) Noise (standard deviation) to signal ratio as in Fig. 3 but for the P_- case.

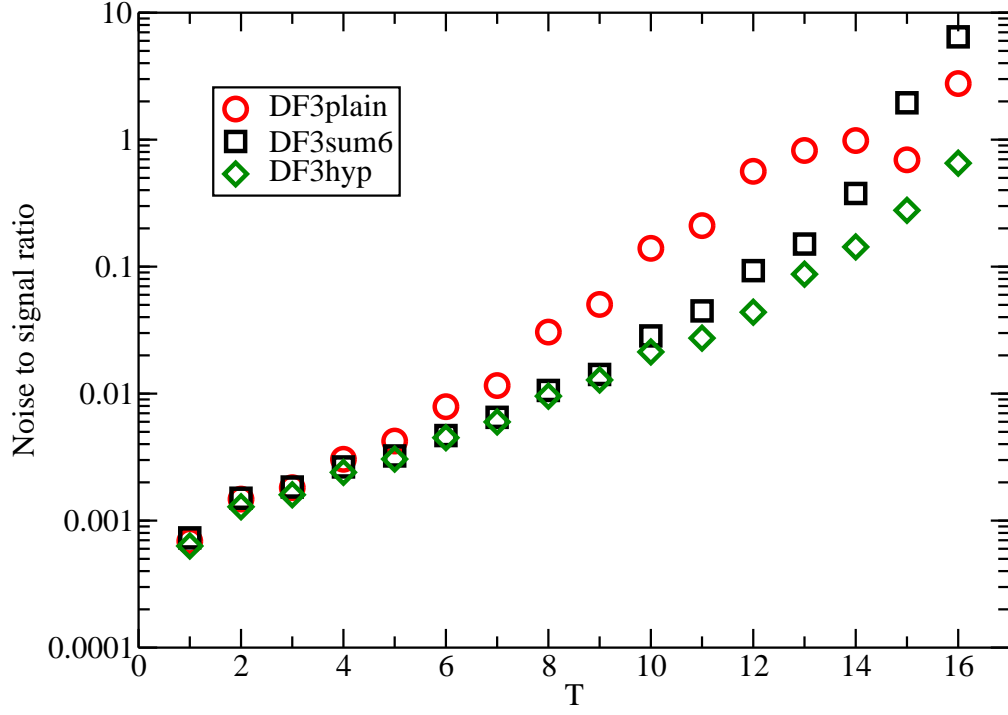


FIG. 5: (Color online) Noise (standard deviation) to signal ratio for the P_+ case.

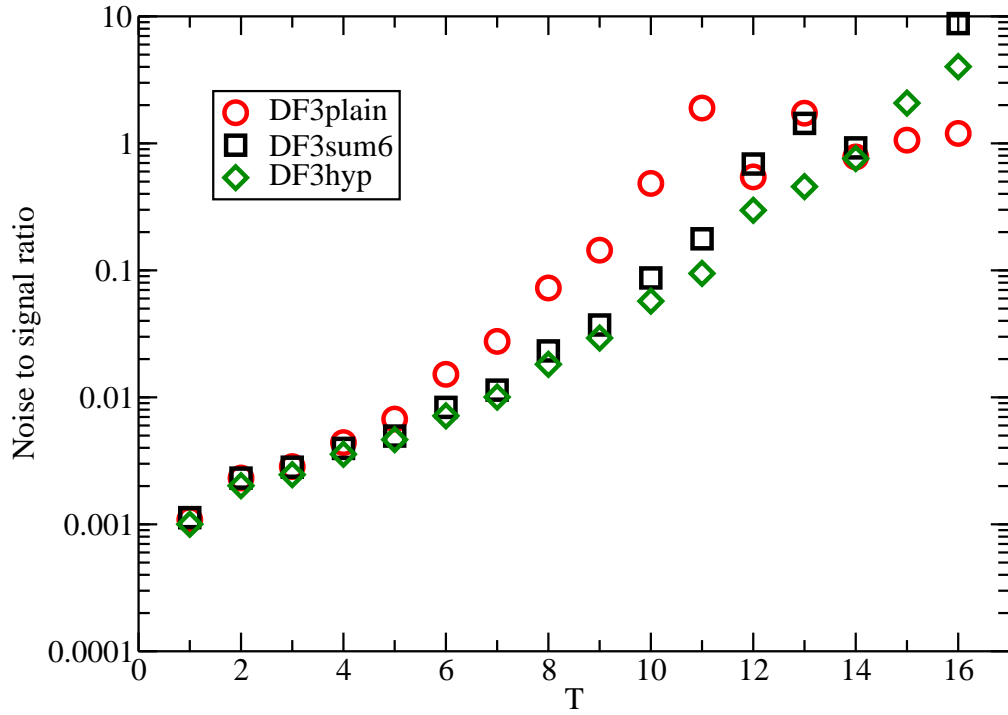


FIG. 6: (Color online) Noise (standard deviation) to signal ratio for the D_- case.

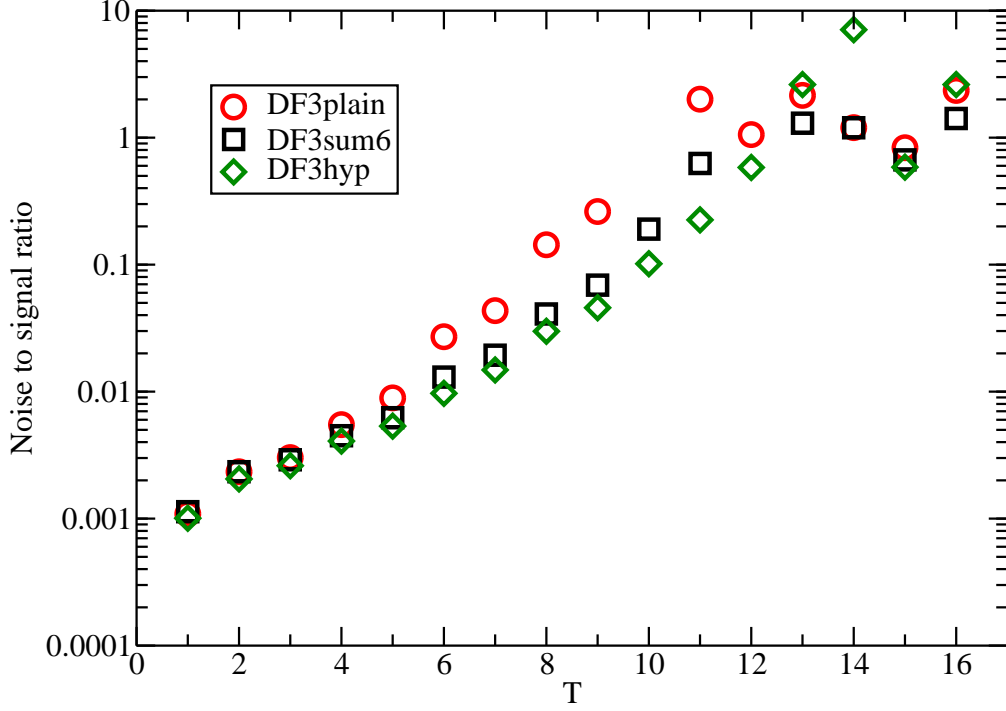


FIG. 7: (Color online) Noise (standard deviation) to signal ratio for the D_+ case.

L_{\pm}	m_1	m_2	m_3	$a_{1,F1}$	$a_{1,F2}$	$a_{2,F1}$	$a_{2,F2}$	$a_{3,F1}$	$a_{3,F2}$	$\frac{\chi^2}{\text{d.o.f.}}$
S	0.527(5)	0.98(2)	1.40(2)	0.297(11)	0.44(2)	1.24(5)	1.56(4)	1.81(5)	0.03(11)	21/24
P_-	0.766(14)	1.29(3)	1.52(3)	0.65(5)	0.93(7)	3.4(3)	2.2(2)	-1.5(6)	3.4(6)	19/24
P_+	0.76(2)	1.28(3)	1.46(2)	0.62(7)	0.88(10)	3.6(4)	3.14(15)	-2.8(5)	2.6(5)	11/24
D_{+-}	1.10(8)	1.46(5)	1.66(6)*	1.0(3)	2.0(5)	5.3(8)	1.8(9)	-0.6(17)	5.1(13)	22/24
D_-	1.01(3)	1.52(2)	1.67(4)*	1.10(14)	2.0(2)	7.2(5)	1.5(12)	-1.4(15)	7.4(8)	36/27
D_+	1.06(2)	1.558(8)	1.80(2)*	1.14(9)	2.09(11)	6.52(6)	-0.5(5)0	1.3(7)	7.6(2)	39/27
F_{+-}	1.20(2)	1.658(5)	1.892(13)*	0.77(8)	1.88(10)	5.30(13)	-1.1(5)	1.3(7)	6.0(3)	37/27

TABLE II: Two-point correlation function fits (equation 2) for “DF3hyp”. 2 path fit results are shown for all states to make comparisons easier, even though our best fits for the S and P_- states are 5 path fits. In some cases (entries marked with an asterisk) Bayesian ideas are used (see section VB). The errors on the parameters were obtained by bootstrapping the lattice configurations and repeating the fit 100 times. The m_i are in lattice units. Note that the $\frac{\chi^2}{\text{d.o.f.}}$ is larger for the D-wave and F-wave states than for the S- and P-wave states.

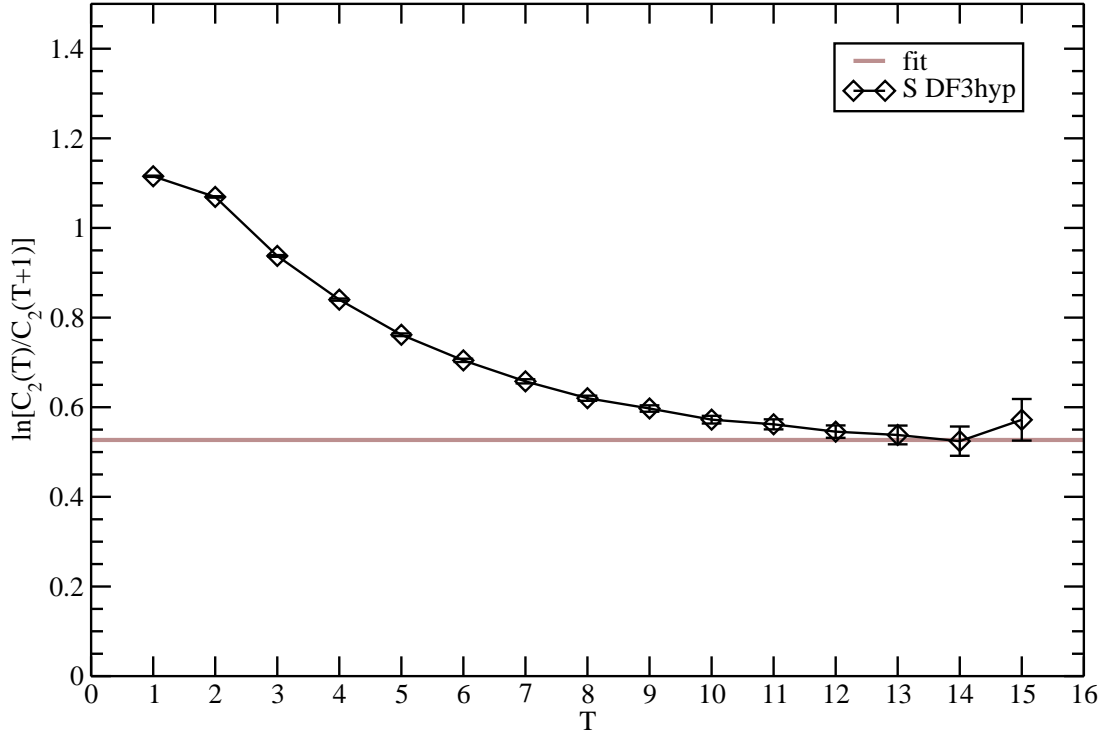


FIG. 8: (Color online) Effective mass plot for the S-wave F2F2 correlations. The line labelled “fit” (here and in the other effective mass plots) shows the lowest energy obtained from the fit in Eq. 2 for the lattice “DF3hyp”. Only 2 paths are used in the fit shown here to make comparisons easier, although the best fit for the S-wave state uses all 5 paths. The thickness of the line indicates the error. As expected from a variational argument, this fit to all data naturally gives a somewhat smaller mass than a fit to F2F2 alone.

V. ENERGY SPECTRUM

The energies are obtained from the fit in equation 2 — see Table II for the results for the lattice “DF3hyp”. The m_i are in lattice units. However, due to the presence of an unknown (but L_\pm and i independent) self energy in each m_i , only the differences $m_i(L_\pm) - m_1(S)$ are relevant. The ground state energy from the 2-path fit for a given state is compared with the effective mass in Figs. 8-12. To illustrate how plateaux develop with T , $\ln [C_2(T)/C_2(T + 1)]$ is shown for the largest component, F2F2, for the same lattice “DF3hyp”. It is seen that for all states we get a plateau that agrees nicely with the fit result that uses all components, F1F1, F1F2 and F2F2. The errors are large for large T values, and the data points for the highest T values are not shown if the errors render them insignificant. In the fits this is

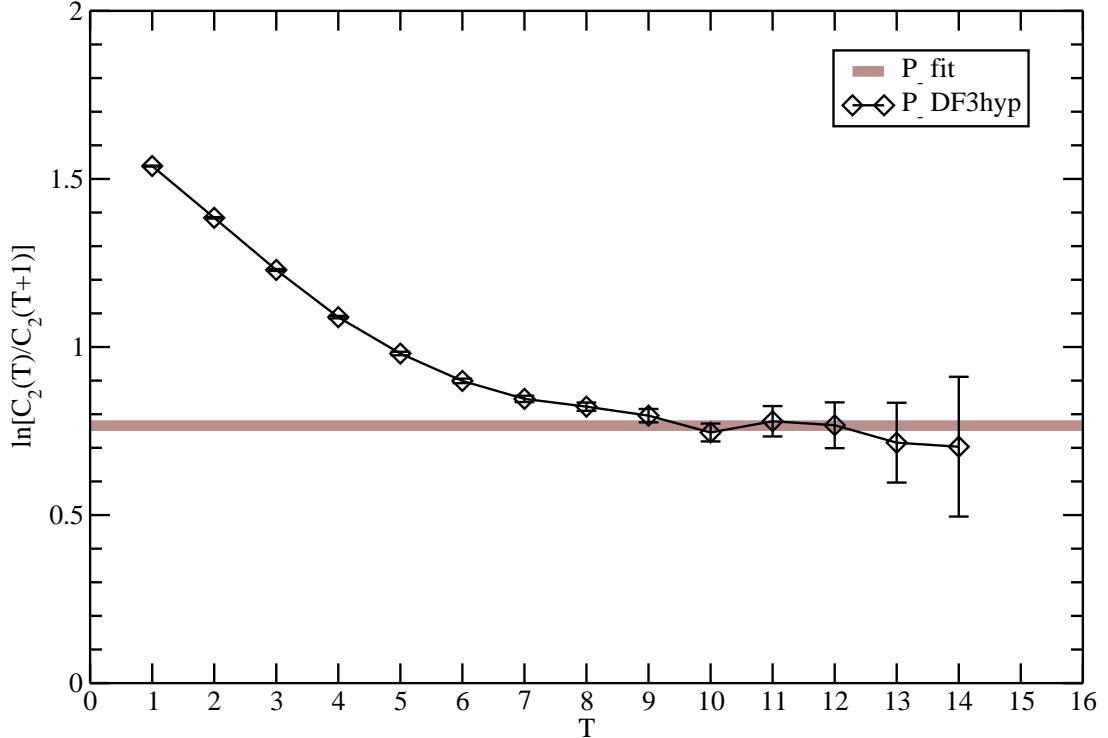


FIG. 9: (Color online) Effective mass plot for the P_- F2F2 correlations. Only 2 paths are used in the fit shown here to make comparisons easier, although the best fit for this state uses all 5 paths. Other details as in Fig. 8.

under better control, because we fit $C_2(T)$ and not the ratio, and all fuzzing combinations are used (i.e. more data are used). We can thus use data up to $T = 15$ in the fits. The fit shown in these figures is only to the 2 path data, to make comparisons easier. When extracting the energy of a state all 5 paths are used for S and P_- . For other states only 2 path data are available.

The resulting energy spectra from the fit (Eq. 2) for different lattices are shown in Figs. 14–16 — see also Tables III–V. With the lattice “DF3”, for most states, using different smearing for the heavy quark does not seem to change significantly the energy differences with respect to the $1S$ energy — the exceptions being the P_+ and excited D_{+-} states. Different smearings should only give the same results in the continuum limit, so it is understandable that at a fixed lattice spacing the results may differ. Unfortunately, all our lattices have approximately the same lattice spacing (about $a = 0.1$ fm, see Table I), and we can not go to the continuum limit properly. However, we can use the results from different smearings

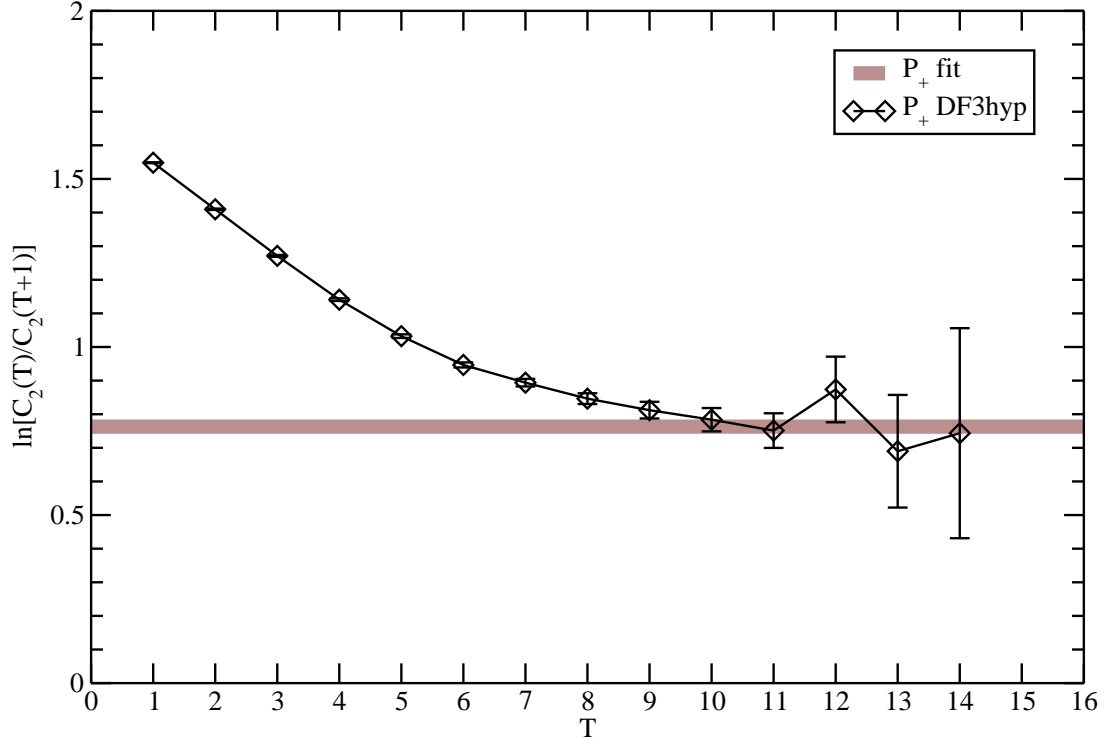


FIG. 10: (Color online) Effective mass plot for the P₊ F2F2 correlations. Other details as in Fig. 8.

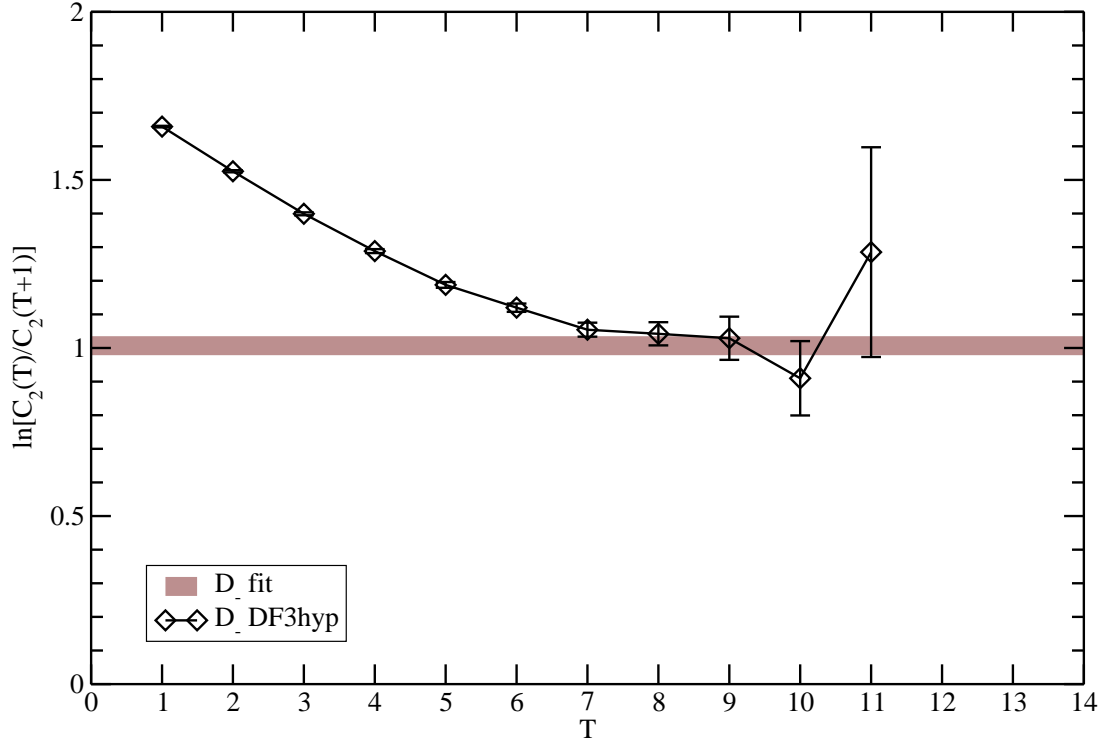


FIG. 11: (Color online) Effective mass plot for the D₋ F2F2 correlations. Other details as in Fig. 8.

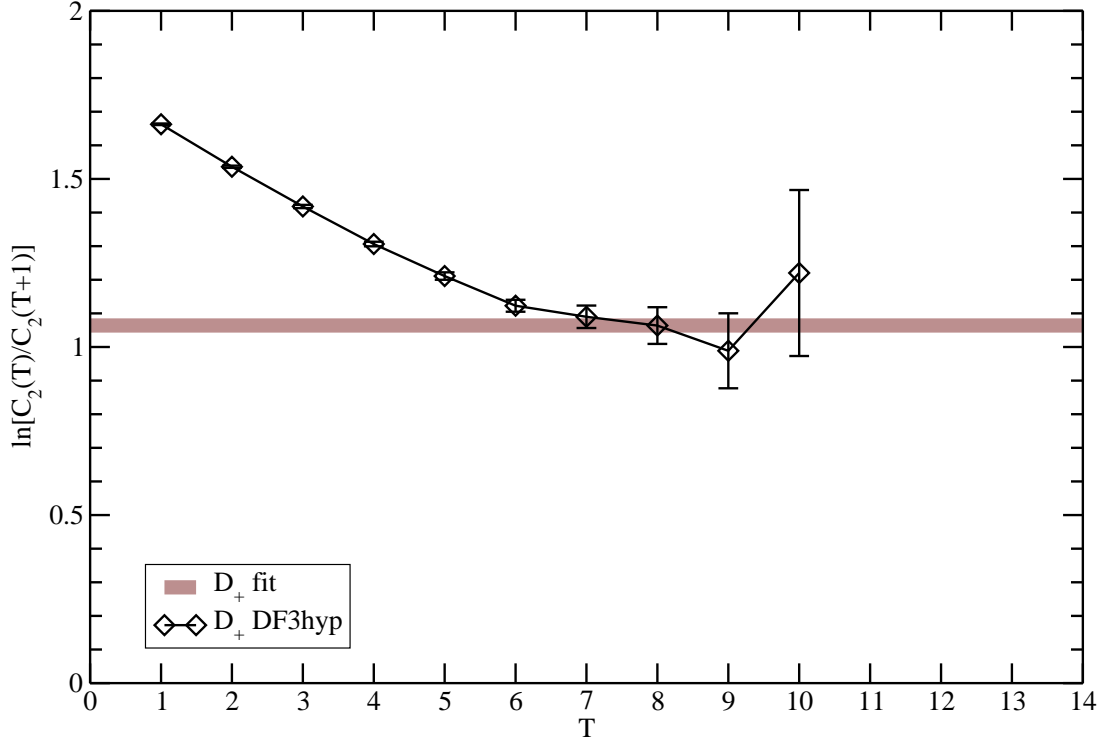


FIG. 12: (Color online) Effective mass plot for the D_+ F2F2 correlations. Other details as in Fig. 8.

to give a rough estimate of the systematic error. Because studying the noise to signal ratio (Figs. 3–7) shows that the “plain” configurations are clearly inferior to the configurations that are smeared in the time direction, we use “hyp” and “sum6” configurations to get our main results. The reason for quoting energies in units of r_0 is to avoid the 5% uncertainty in $r_0 = 0.525(25)$ fm. The uncertainties in r_0/a are much smaller. To get energies in GeV then requires an additional factor of $0.38(2)$.

The energy of the D_{+-} state had been expected to be near the spin average of the D_- and D_+ energies, but it turns out to be a poor estimate of this average. Therefore, it is not clear to what extent the F_{+-} energy is near the spin average of the two F-wave states, as was originally hoped. The F- and D-wave results for different smearings for the lattices “DF4” and “DF5” are somewhat more scattered than for the “DF3” lattice (i.e. the systematic errors are larger), but otherwise the same features are seen for all three light quark masses. We are most interested in the “DF3” lattice results, because that is closest to the B_s meson (the light quark mass on this lattice being close to the s quark mass). One interesting observation is, that the energy spectrum is close to being dependent on L alone.

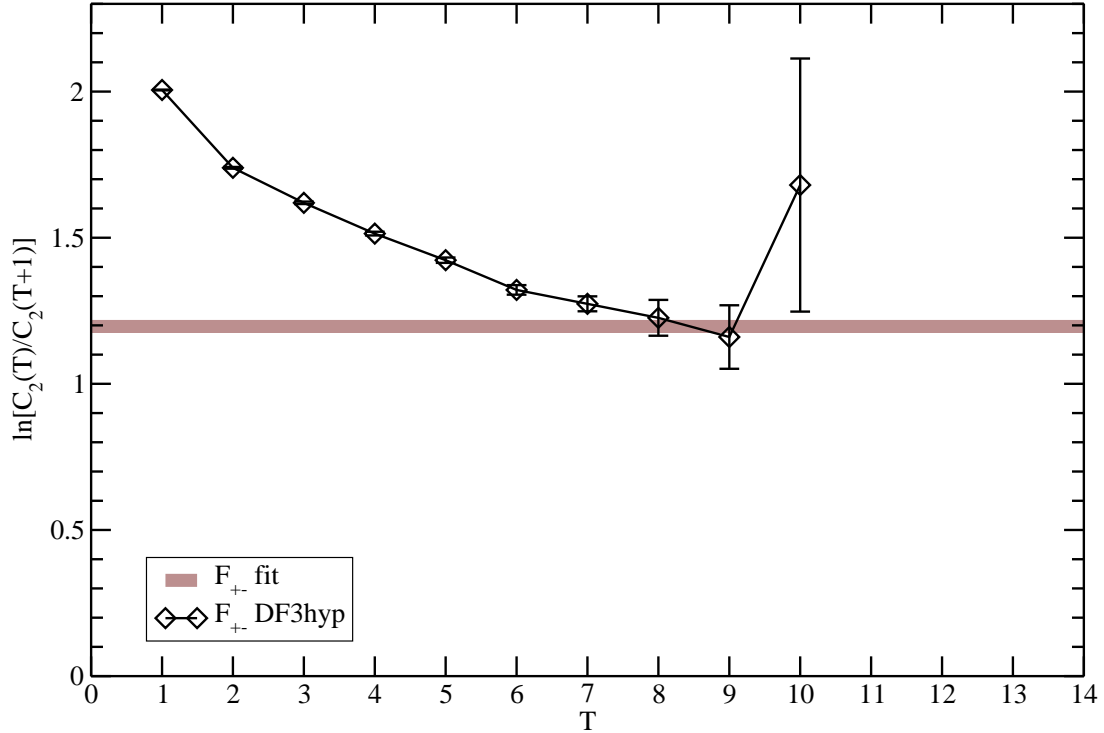


FIG. 13: (Color online) Effective mass plot for the F_{+-} F2F2 correlations. Other details as in Fig. 8.

For example our preferred configurations, “DF3hyp”, show an approximate linear rise in excitation energy with L (up to F-wave) as $\sim 0.4L$ GeV. A similar linear rise is usually seen in Regge or string models. In contrast, the 2S state is seen to be almost degenerate with the 1D states, as in a simple harmonic oscillator. A $L(L+1)$ term can be added to the linear ansatz to get a better fit — more precisely, $0.34L+0.04L(L+1)$ gives a good overall fit to the four energy differences up to D-waves.

Our earlier results (for the “plain” configurations used in this study as well as for some other unquenched and quenched configurations) can be found in Refs. [2, 7]. Because dynamical fermions are used in this study, we can not be absolutely certain that the lattice states are pure quark–anti-quark states. However, our radial distribution measurements [8] support the assumption that the states are ordinary meson states: the radial distributions of the lowest lying states are not broad, as would be the case if the states were molecules, and the first radial excitations of S- and P-wave states have one node at short distances (approximately at 0.30–0.35 fm).

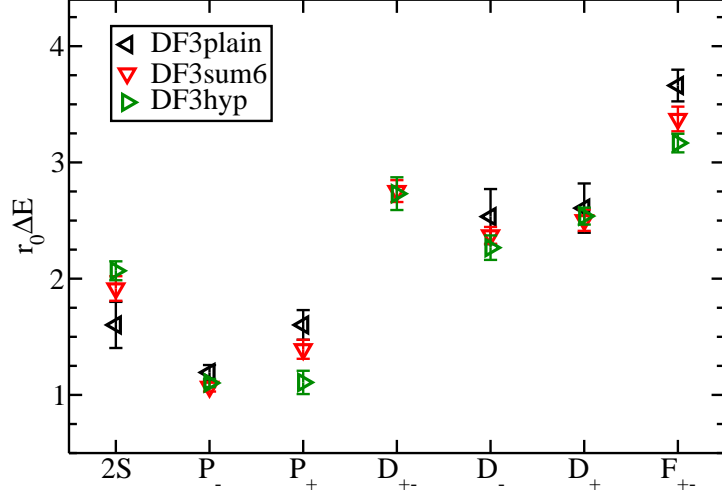


FIG. 14: (Color online) Energy spectrum of the heavy-light meson using lattice “DF3” in units of r_0 . Here $L_+(-)$ means that the light quark spin couples to angular momentum L giving the total $j = L \pm 1/2$. The 2S is the first radially excited $L=0$ state. The D_{+-} is a mixture of the D_- and D_+ states, and likewise for the F_{+-} . Energies are given with respect to the S-wave ground state (1S). Here $r_0/a = 4.754(40)^{+2}_{-90}$ (from [1]). The error bars shown here contain only the statistical errors on the lattice energy fits.

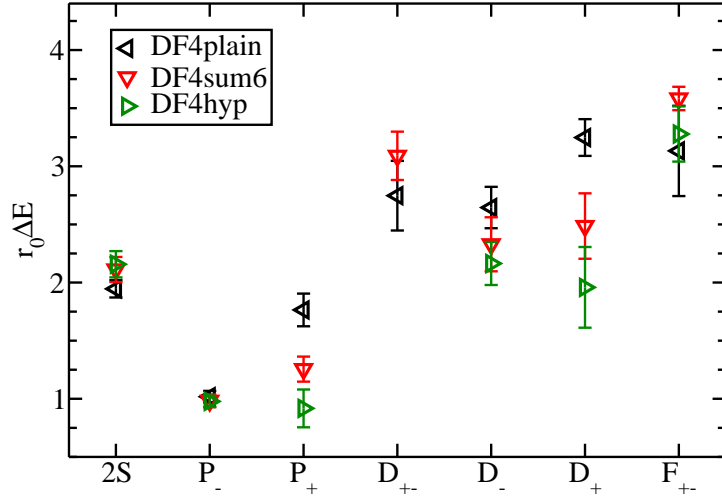


FIG. 15: (Color online) Energy spectrum of the heavy-light meson using lattice “DF4”. See Fig. 14 for details. Here $r_0/a = 5.041(40)^{+0}_{-10}$ (from [1]). The error bars shown here contain only the statistical errors on the lattice energy fits.

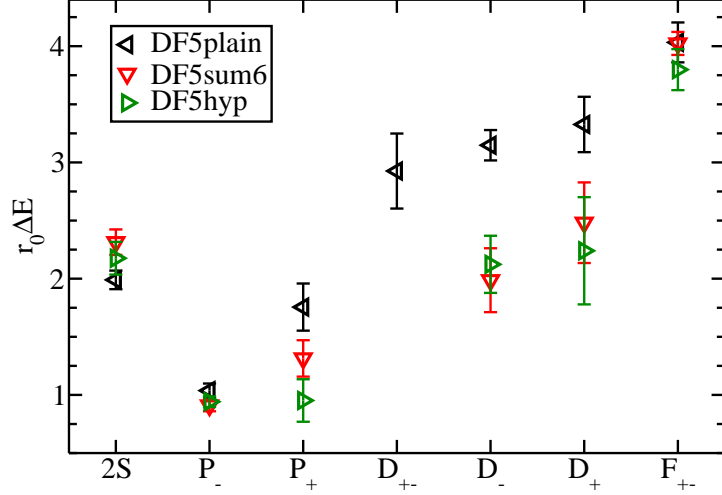


FIG. 16: (Color online) Energy spectrum of the heavy-light meson using lattice “DF5”. See Fig. 14 for details. Here $r_0/a = 5.32(5)$ (from [1]). The error bars shown here contain only the statistical errors from the lattice energy fits.

nL _±	DF3plain	DF3sum6	DF3hyp	nL _±	DF3plain	DF3sum6	DF3hyp
1S	3.55(6)	2.724(14)	2.520(10)	2S	5.1(2)	4.64(10)	4.59(8)
1P ₋	4.74(3)	3.79(4)	3.62(3)	2P ₋	7.13(5)	5.98(10)	5.97(10)
1P ₊	5.15(11)	4.12(8)	3.63(10)	2P ₊	7.80(9)	6.62(8)	6.1(2)
1D ₊₋	-	5.48(9)	5.25(14)	2D ₊₋	-	6.88(4)	7.05(7)
1D ₋	6.1(2)	5.10(7)	4.79(13)	2D ₋	8.44(14)	7.50(4)	7.23(11)
1D ₊	6.2(2)	5.23(9)	5.06(7)	2D ₊	8.38(15)	7.59(5)	7.41(4)
1F ₊₋	7.21(12)	6.10(11)	5.69(8)	2F ₊₋	9.16(3)	8.18(3)	7.88(2)

TABLE III: Heavy-light meson energies on the lattice in units of r_0 for “DF3”. The uncertainty due to the statistical error on r_0/a [$r_0/a = 4.754(40)_{-90}^{+2}$, from [1]] is small (less than 1%), and is not taken into account in the error estimates. The n denotes the radial excitation and n−1 gives the number of nodes in the wavefunction of the state. The dash means that no reliable fit can be found. The results on different lattices can not be compared directly (only energy differences can be compared) due to different self energies. The “DF3hyp” results are the same as m_1, m_2 in Table II, but expressed in different units. Also the 1S, 1P₋ are now from 5 path fits.

nL_{\pm}	DF4plain	DF4sum6	DF4hyp	nL_{\pm}	DF4plain	DF4sum6	DF4hyp
1S	3.72(4)	2.66(2)	2.45(2)	2S	5.66(7)	4.77(11)	4.61(11)
1P ₋	4.73(4)	3.64(5)	3.43(5)	2P ₋	7.38(6)	6.03(12)	5.91(11)
1P ₊	5.48(14)	3.92(11)	3.37(16)	2P ₊	8.27(11)	6.65(9)	6.0(2)
1D ₊₋	6.5(3)	5.8(2)	-	2D ₊₋	8.24(12)	7.25(9)	-
1D ₋	6.4(2)	5.0(2)	4.6(2)	2D ₋	8.91(8)	7.6(2)	7.2(2)
1D ₊	6.96(15)	5.1(3)	4.4(3)	2D ₊	9.16(8)	7.9(2)	7.1(2)
1F ₊₋	6.8(4)	6.24(10)	5.7(2)	2F ₊₋	9.51(11)	8.62(2)	8.33(10)

TABLE IV: Heavy-light meson energies on the lattice in units of r_0 for “DF4”. The uncertainty due to the statistical error on r_0/a [$r_0/a = 5.041(40)_{-10}^{+0}$, from [1]] is small (less than 1%), and is not taken into account in the error estimates. Other comments as in Table III.

nL_{\pm}	DF5plain	DF5sum6	DF5hyp	nL_{\pm}	DF5plain	DF5sum6	DF5hyp
1S	3.71(5)	2.70(3)	2.46(3)	2S	5.70(6)	5.01(11)	4.63(14)
1P ₋	4.75(4)	3.61(4)	3.40(4)	2P ₋	7.57(6)	6.23(10)	6.11(10)
1P ₊	5.5(2)	4.01(15)	3.4(2)	2P ₊	8.51(12)	6.96(11)	6.3(2)
1D ₊₋	6.6(3)	-	-	2D ₊₋	8.71(13)	-	-
1D ₋	6.86(12)	4.7(3)	4.6(2)	2D ₋	9.51(5)	7.5(2)	7.4(2)
1D ₊	7.0(2)	5.2(3)	4.7(5)	2D ₊	9.61(8)	8.2(2)	7.6(3)
1F ₊₋	7.7(2)	6.72(10)	6.3(2)	2F ₊₋	10.05(6)	9.01(3)	8.6(3)

TABLE V: Heavy-light meson energies on the lattice in units of r_0 for “DF5”. The uncertainty due to the statistical error on r_0/a [$r_0/a = 5.32(5)$, from [1]] is small (less than 1%), and is not taken into account in the error estimates. Other comments as in Table III.

To check how the results depend on the light quark mass we plot the energies (i.e. energy differences with respect to the 1S state) as a function of the pion mass squared, $(r_0 m_{\pi})^2$. As can be seen in Figs. 17–20, for P- and D-wave states the dependence on the light quark mass is not strong. We also compare our results to other static-light meson lattice calculations in Fig. 21. It is seen that the P-wave results do not change much between the different lattices, but the 2S-1S and D-wave energy differences vary a lot. However, since the lattices, quark masses and lattice spacings are different, the results should only agree in the continuum

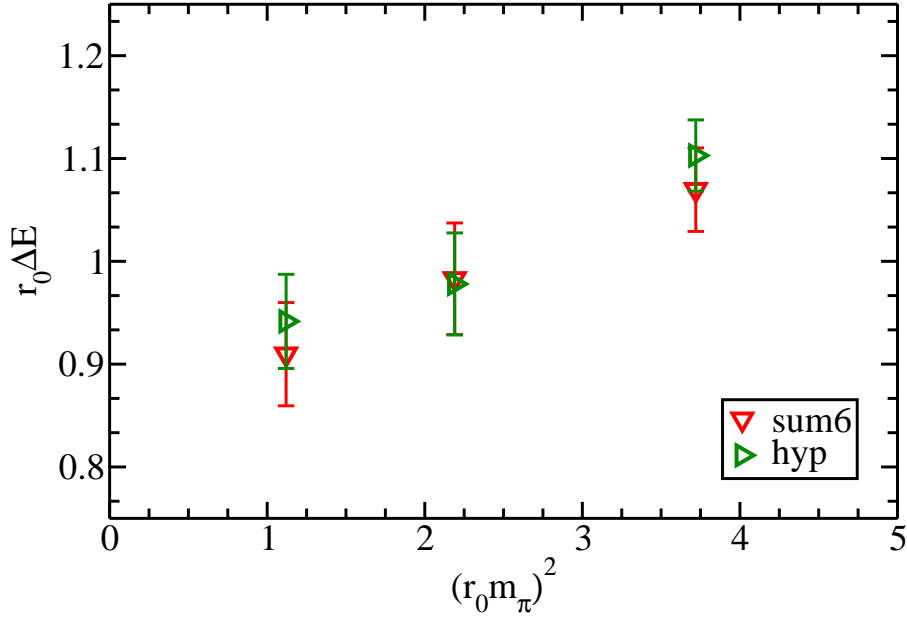


FIG. 17: (Color online) The energy difference $r_0[E(1P_-)-E(1S)]$ as a function of the pion mass squared. There is a slight dependence on the light quark mass. Here and in the following figures for P_+ , D_- and D_+ the results, from left to right, are from lattices “DF5”, “DF4” and “DF3”, respectively.

limit. A set of similar lattices with different lattice spacings would be needed to check this.

A. Interpolation to the b quark mass

Even though we can not go to the continuum limit, we feel that it is worth-while to try to predict where the B_s meson excited states lie. To obtain the predictions of the excited state energies, we can now interpolate in $1/m_Q$, where m_Q is the heavy quark mass, between the “DF3” heavy-light lattice calculations and D_s meson experimental results, i.e. interpolate between the static quark ($m_Q = \infty$) and the charm quark ($m_Q = m_c$). Here we, of course, have to assume that the measured D_s meson states are simple quark–anti-quark states. This is not necessarily true: for example the mass of the $D_{s0}^*(2317)$ is much lower than what is predicted by conventional potential models, and it has thus been proposed that it could be either a four quark state, a DK molecule or a $D\pi$ atom. A short review on meson excited state spectroscopy and the puzzles in interpreting the results is given in Ref. [13]. However, the inclusion of chiral radiative corrections could change the potential model predictions

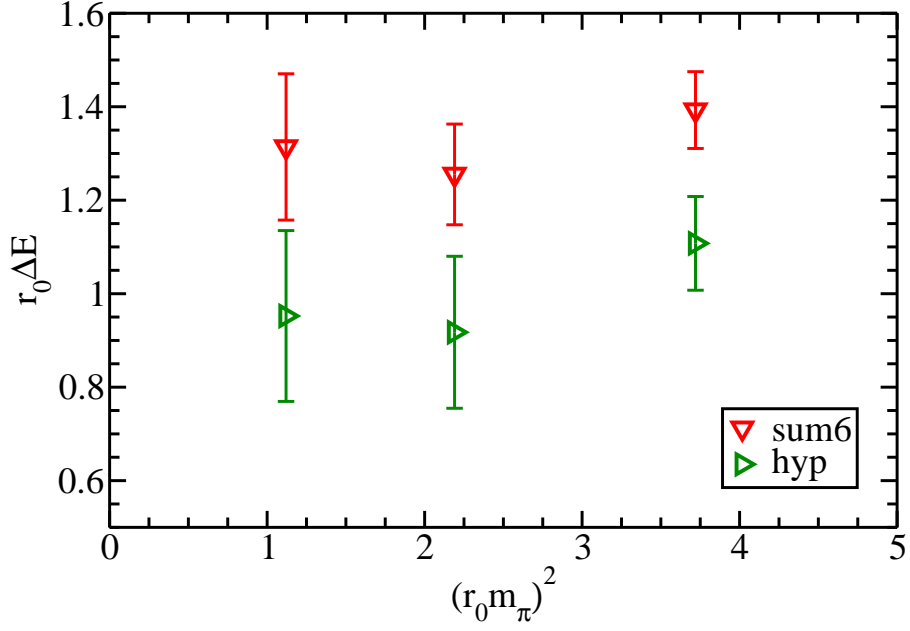


FIG. 18: (Color online) The energy difference $r_0[E(1P_+) - E(1S)]$ as a function of the pion mass squared. The dependence on the light quark mass is weak, whereas there is a manifest difference between “sum6” and “hyp” configurations.

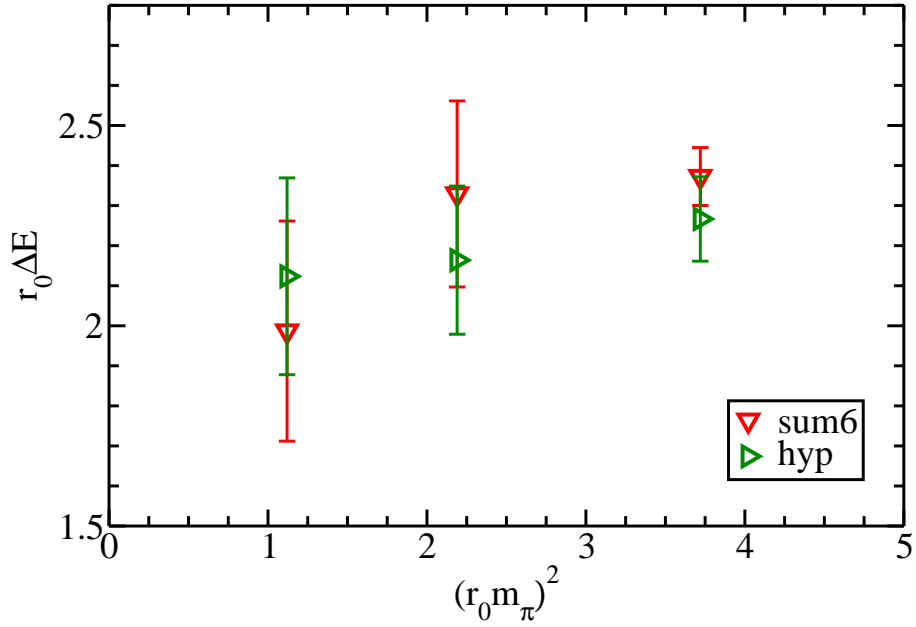


FIG. 19: (Color online) The energy difference $r_0[E(1D_-) - E(1S)]$ as a function of the pion mass squared. The dependence on the light quark mass is weak, and the differences between the “sum6” and “hyp” smearings are small — especially for “DF3”.

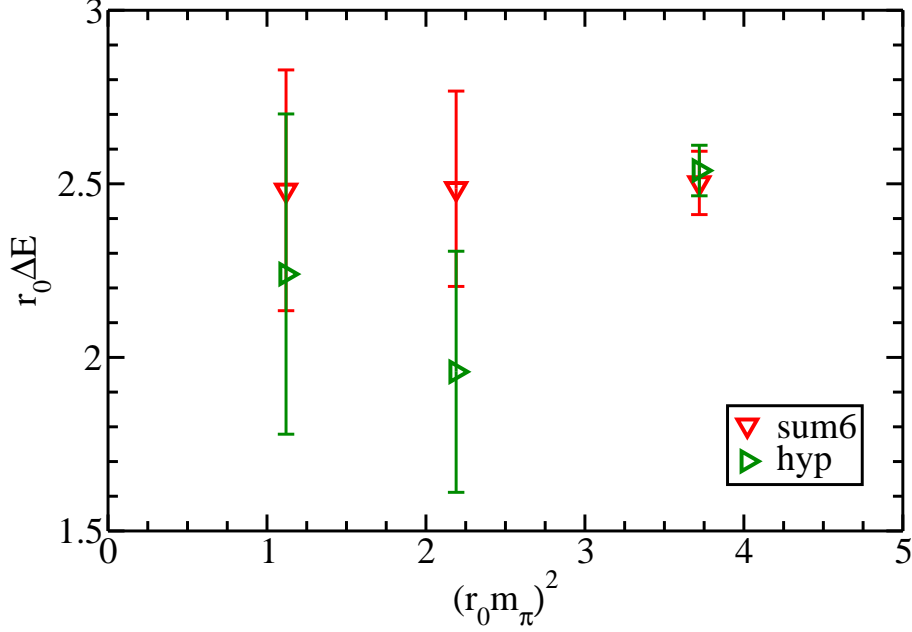


FIG. 20: (Color online) The energy difference $r_0[E(1D_+) - E(1S)]$ as a function of the pion mass squared. The dependence on the light quark mass is weak, and the differences between the “sum6” and “hyp” smearings are small — especially for “DF3”.

considerably [14]. In the following we assume that the states are the usual quark–anti-quark states.

We use linear interpolation, i.e.

$$\Delta E = A + B \frac{m_c}{m_Q} + C F_j \frac{m_c}{m_Q}. \quad (6)$$

Here A , B and C are fit parameters and $F_j = 2[J(J+1) - j_q(j_q+1) - s_Q(s_Q+1)]$, where J is the total angular momentum, $s_Q = 1/2$ is the heavy quark spin and j_q is the combined spin and orbital angular momentum L of the light quark (see Table VI). The interpolation procedure is shown in Fig. 22. Note that the linear interpolation works perfectly for the 1^- S-wave state, where the experimental energies are known for both B_s and D_s mesons, and the lattice result (zero) is simply because the two 1S states are automatically degenerate at $m_Q = \infty$.

Our predictions of the energy differences $m(1P) - m(1S)$ for the B_s meson are given in Table VII. For our preferred lattice “DF3hyp” these agree very well with the experimental measurements of the energies of the 1^+ and 2^+ P-wave states. There we predict that the two lowest P-wave states lie a few MeV below the BK and B^*K thresholds (minus the 1S state

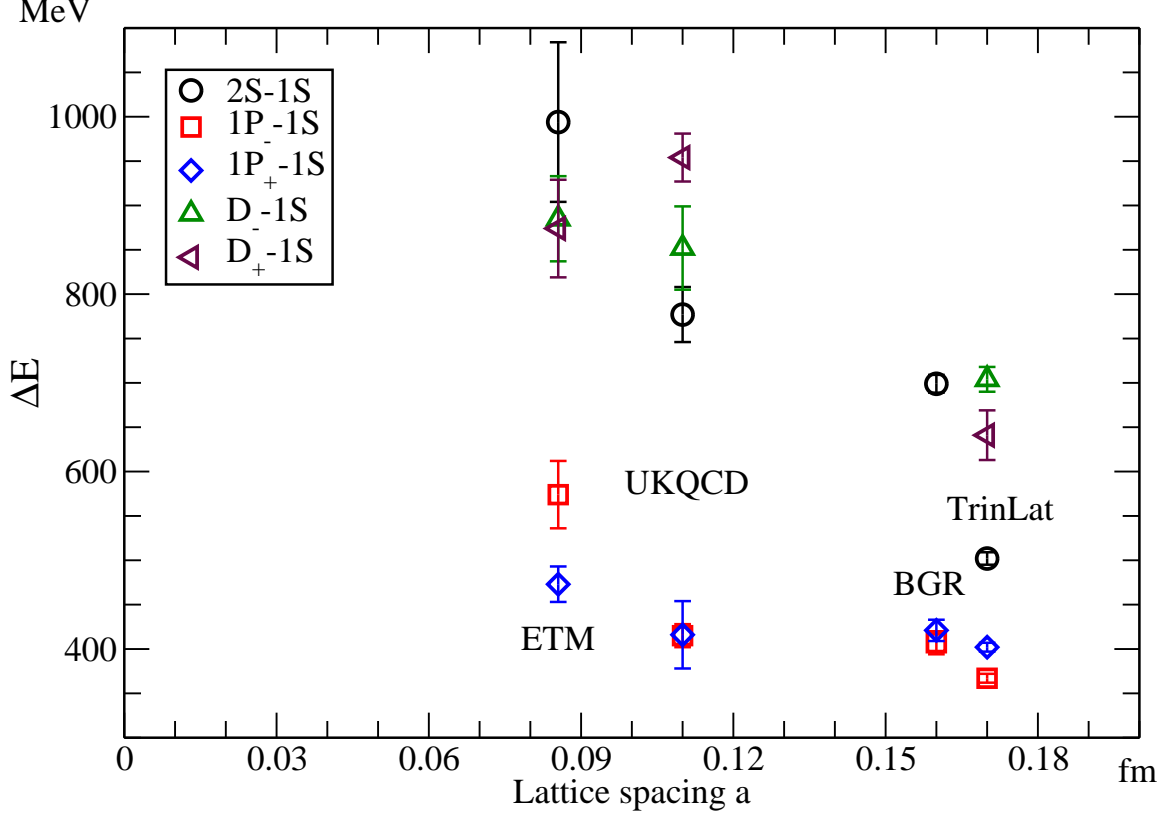


FIG. 21: (Color online) Comparison of different static-light lattice results. On the left at $a = 0.0855$ fm are the results from European Twisted Mass Collaboration [9], at $a = 0.11$ fm our results, at $a = 0.16$ fm BGR Collaboration’s results [10] and on the right at $a = 0.17$ fm TrinLat group’s results [15]. A set of similar lattices with different lattice spacings is needed for going to the continuum limit.

J^P L F_j	J^P L F_j	J^P L F_j
0^+ 0 -3	0^+ 1 -3	1^+ 1 -5
1^+ 0 +1	1^+ 1 +1	2^+ 1 +3

TABLE VI: Coefficients $F_j = 2[J(J+1) - j_q(j_q+1) - s_Q(s_Q+1)]$ (equation 6).

energy) at 406 and 452 MeV respectively. We show the “DFsum6” results for comparison.

As for other excited states, BaBar and Belle observed two new states, $D_{sJ}^*(2860)$ and $D_{sJ}^*(2700)$, in 2006 [16, 17]. The J^P quantum numbers of the $D_{sJ}^*(2860)$ can be 0^+ , 1^- , 2^+ , etc., so it could be a radial excitation of the $D_{s0}^*(2317)$ or a $J^P = 3^-$ D-wave state. The first interpretation is rather popular, but our lattice results favor the D-wave $J^P = 3^-$ assignment in agreement with Colangelo, De Fazio and Nicotri [18]. (The slope of the interpolating line

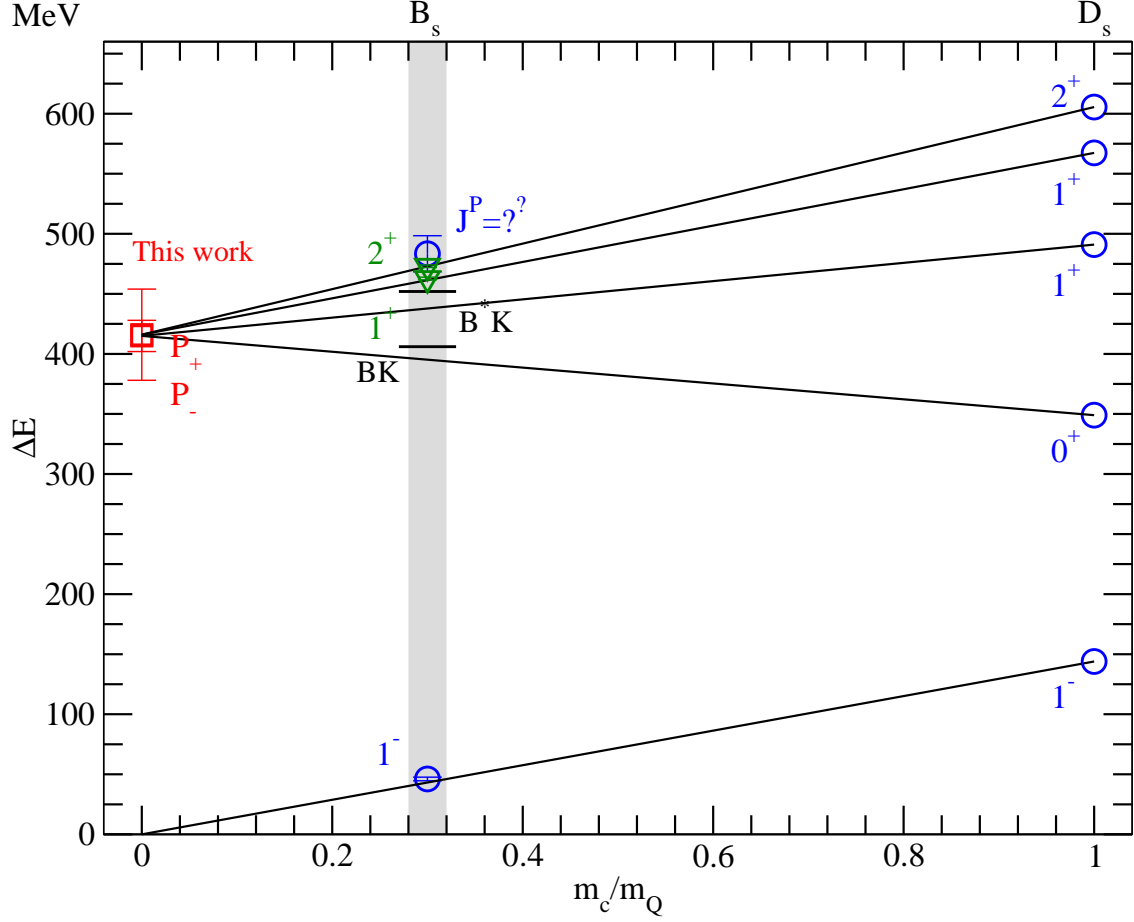


FIG. 22: (Color online) Interpolation to the b quark mass. The ratio m_c/m_b is taken to be 0.30(2) (from [11]; shown by the vertical band). The D_s meson experimental results are from [11] (blue circles), and the B_s meson experimental results are from [11] (blue circles) and [12] (green triangles). Our results (using “DF3hyp” configurations) are marked with red squares.

J^P	DF3hyp	DF3sum6	experiments
0^+	393 ± 9 MeV	384 ± 10 MeV	-
1^+	440 ± 9 MeV	432 ± 10 MeV	-
1^+	466 ± 25 MeV	538 ± 21 MeV	463 ± 1 MeV
2^+	482 ± 25 MeV	551 ± 21 MeV	473 ± 1 MeV

TABLE VII: Our predictions for B_s meson mass differences, $M(B_s^*) - M(B_s)$, for the P-wave states. The uncertainty in the ratio m_c/m_b is not taken into account in the error estimates. The experimental results are from [12].

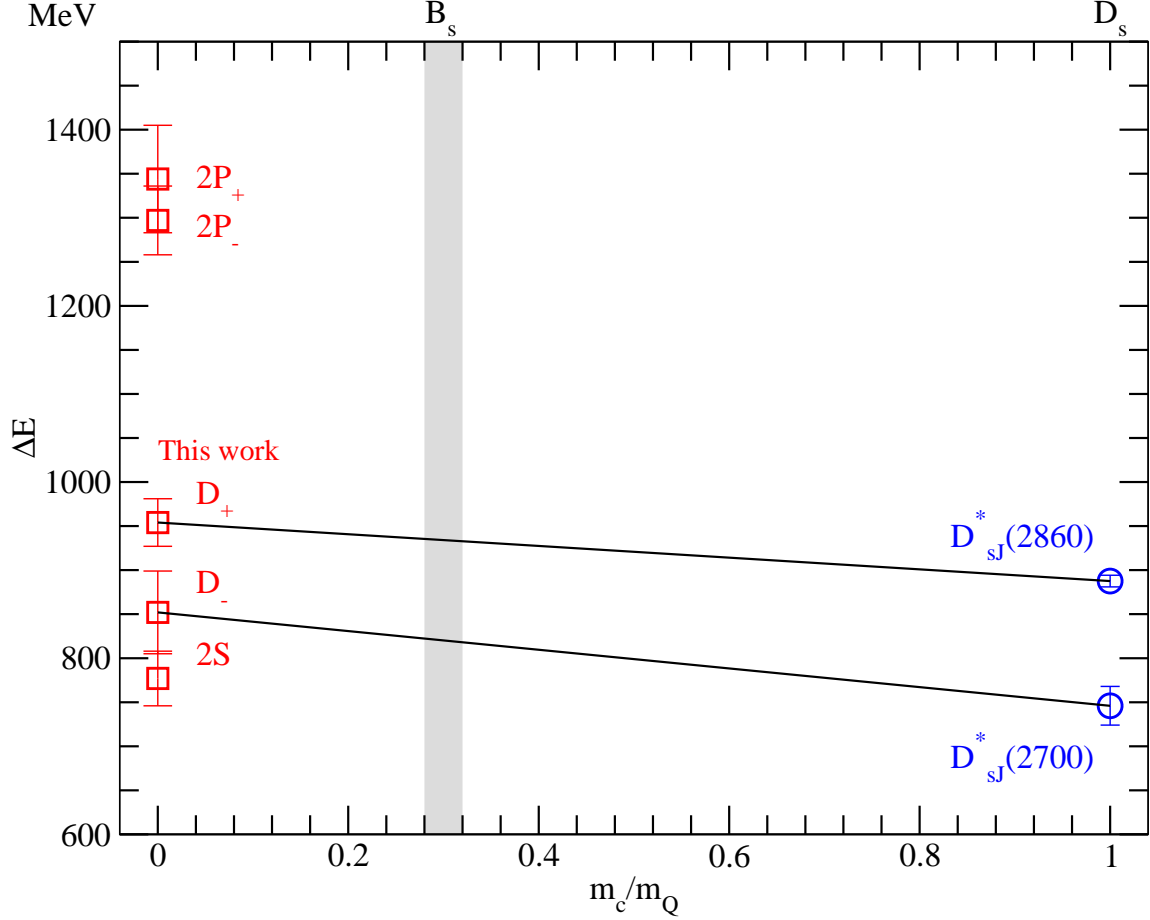


FIG. 23: (Color online) Interpolation to the b quark mass for “DF3hyp” lattice: higher excited states. The lines illustrate what the interpolation would look like, if the D_s meson states were D-wave states. The experimental results are from [16, 17]. Interpolating to m_c/m_b predicts D-wave $J^P = 1^-, 3^-$ at 817(31) and 932(18) MeV respectively.

would be very steep, if the $D_{sJ}^*(2860)$ is a radial excitation of the $D_{s0}^*(2317)$.) Interpolation then predicts a D-wave $J^P = 3^-$ B_s state at 932(18) MeV. In addition, the $D_{sJ}^*(2700)$ could be a radially excited S-wave state or a D-wave $J^P = 1^-$ state. If the latter identification is assumed, then a D-wave $J^P = 1^-$ B_s state at 817(31) MeV is expected (see Fig. 23).

B. Bayesian ideas

In some cases, using 3 exponentials to fit the C_2 data does not work very well. In Table II, these cases are marked with an asterisk. Since these fits are not as good or stable as one would hope, we introduce some Bayesian ideas and use prior knowledge of the energies to

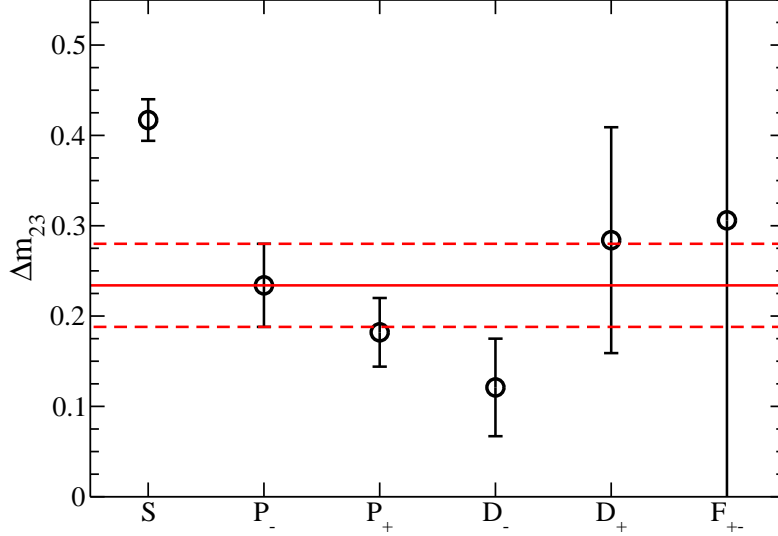


FIG. 24: (Color online) Mass differences $\Delta m_{32} = m_3 - m_2$ for the “DF3hyp” data in lattice units. This seems to be almost constant for angular momentum $L \geq 1$ (given the sizeable errors on the data). The lines give the $\Delta m_{32} = 0.234(46)$ that is used in this study. Looking at the “DF3sum6” data gives a very similar picture (not shown here) and an estimate of $\Delta m_{32} = 0.207(54)$. See section V B for details.

nL_{\pm}	m_3 3 exp	$m_{3, \text{prior}}$	m_3 Bayes	m_2 3 exp	m_2 Bayes
P_+	1.46(2)	1.52(6)	1.471(15)	1.28(3)	1.29(3)
D_-	1.63(5)	1.74(6)	1.67(4)	1.51(3)	1.52(2)
D_+	1.84(12)	1.79(5)	1.80(2)	1.559(11)	1.558(8)
F_{+-}	1.96(43)	1.89(5)	1.89(1)	1.66(2)	1.657(5)

TABLE VIII: Comparison of the $m_{3, \text{prior}}$ with the results from the full 3 exponential fit and the Bayesian fit for “DF3hyp” configurations. See Section V B for definition of $m_{3, \text{prior}}$. “ m_3 3 exp” and “ m_3 Bayes” are the results of a full 3 exponential fit and a Bayesian (fixed m_{32}) fit, respectively. Likewise for the m_2 . The P_+ “Bayes” fit is merely to check that the Bayesian ideas work well and does not restrict the analysis too much.

constrain the fit, or rather to guide the fit in the right direction. The third mass, m_3 , (which would be the mass of the second radial excitation, if there was no pollution from higher states) is restricted to be in the range $m_{3, \text{prior}} \pm \Delta m_{3, \text{prior}}$ by adding a term

$$\frac{(m_3 - m_{3, \text{prior}})^2}{(\Delta m_{3, \text{prior}})^2} \quad (7)$$

nL_{\pm}	m_3 3 exp	$m_{3, \text{prior}}$	m_3 Bayes	m_2 3 exp	m_2 Bayes
P_+	1.59(2)	1.61(5)	1.59(2)	1.39(2)	1.393(15)
D_-	1.80(9)	1.79(5)	1.79(3)	1.578(11)	1.577(8)
D_+	2.1(2)	1.82(5)	1.84(2)	1.604(12)	1.596(11)
F_{+-}	2.6(9)	1.94(6)	1.950(11)	1.72(2)	1.721(8)

TABLE IX: Comparison of the $m_{3, \text{prior}}$ with the results from the full 3 exponential fit and the Bayesian fit for “DF3sum6” configurations. Again, the prior m_3 values are in fairly good agreement with the m_3 results from the full 3 exponential fits. Fixing $m_3 - m_2$ does not change the first excited state m_2 . See Table VIII for notation.

Lattice	Direct	Indirect	Lattice	Direct	Indirect	Lattice	Direct	Indirect
DF3plain	0.26(4)	0.41(12)	DF4plain	0.69(4)	0.75(14)	DF5plain	0.50(6)	0.7(2)
DF3sum6	0.15(4)	0.32(9)	DF4sum6	0.07(5)	0.27(12)	DF5sum6	0.13(6)	0.40(16)
DF3hyp	0.00(4)	0.00(11)	DF4hyp	0.03(5)	-0.06(17)	DF5hyp	0.07(7)	0.0(2)

TABLE X: P-wave spin-orbit splitting $r_0 \Delta E = r_0(m_{1P_+} - m_{1P_-})$ for the different lattices. To get ΔE in GeV requires a factor 0.38(2).

to the χ^2 . This is not a hard constraint, unlike fixing m_3 to a given value would be, but rather constrains the parameter to a given range softly. The $m_{3, \text{prior}}$ and $\Delta m_{3, \text{prior}}$ are determined beforehand by estimating the difference $\Delta m_{32} = m_3 - m_2$ from full 3 exponentials fits. This mass difference seems to be almost constant for states that have $L = 1$ or higher (see Fig. 24). Therefore we use the P_- state to set the Δm_{32} for D-wave and F-wave states. The $m_{3, \text{prior}}$ for D-wave and F-wave states is then calculated by adding Δm_{32} to the m_2 from the full 3 exponential fit for the state in question (see Tables VIII, IX). The prior m_3 values are in fairly good agreement with the m_3 results from the full 3 exponential fits, and fixing $m_3 - m_2$ does not change the first excited state m_2 . The P_+ “Bayes” fit are used to check that the Bayesian ideas work well and does not restrict the analysis too much.

C. Spin-orbit splitting

One interesting point to note here is that the spin-orbit splitting of the P-wave states is small, almost zero, for the preferred “hyp” smearing. We extract this energy difference of

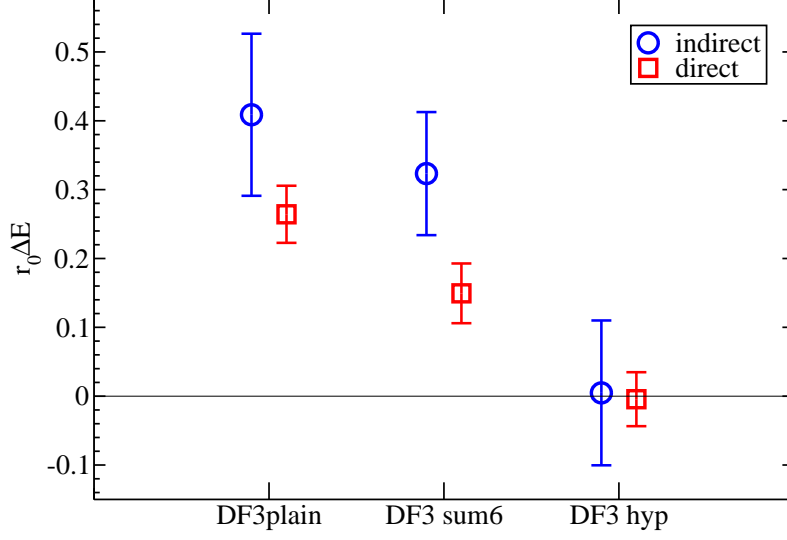


FIG. 25: (Color online) The Spin-Orbit splittings of P-wave states for the “DF3” lattice.

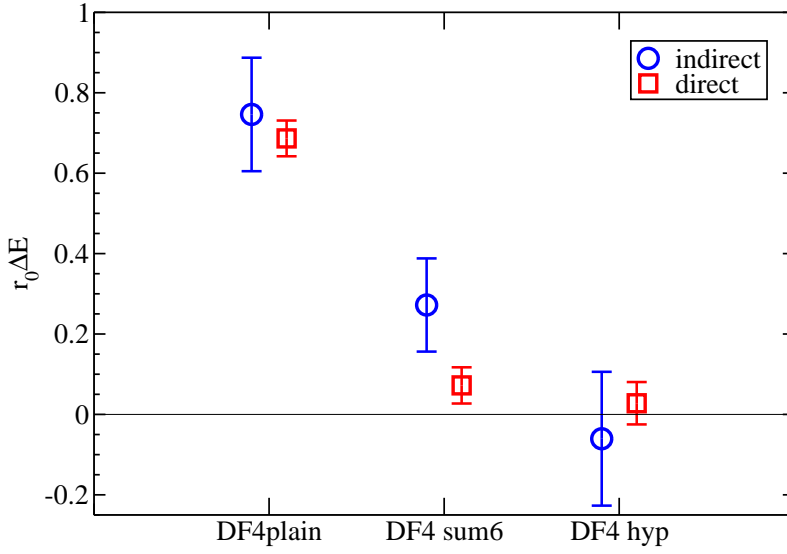


FIG. 26: (Color online) The Spin-Orbit splittings of P-wave states for the “DF4” lattice.

Lattice	Direct	Indirect	Lattice	Direct	Indirect	Lattice	Direct	Indirect
DF3plain	0.13(9)	0.1(3)	DF4plain	0.64(9)	0.6(2)	DF5plain	0.20(10)	0.2(3)
DF3sum6	0.13(3)	0.13(11)	DF4sum6	0.17(6)	0.2(4)	DF5sum6	0.43(5)	0.5(4)
DF3hyp	0.28(5)	0.27(14)	DF4hyp	-0.18(7)	0.2(4)	DF5hyp	0.12(6)	0.1(5)

TABLE XI: D-wave spin-orbit splitting $r_0\Delta E = r_0(m_{1D_+} - m_{1D_-})$ for the different lattices. To get ΔE in GeV requires a factor 0.38(2).

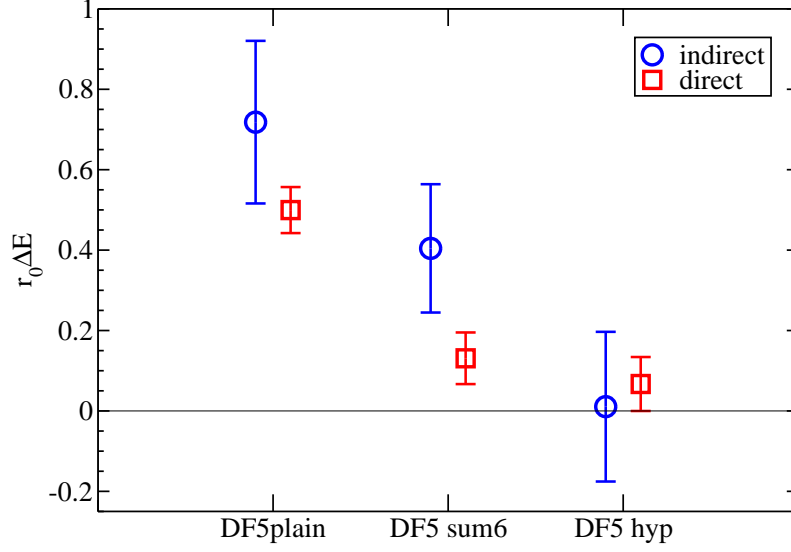


FIG. 27: (Color online) The Spin-Orbit splittings of P-wave states for the “DF5” lattice.

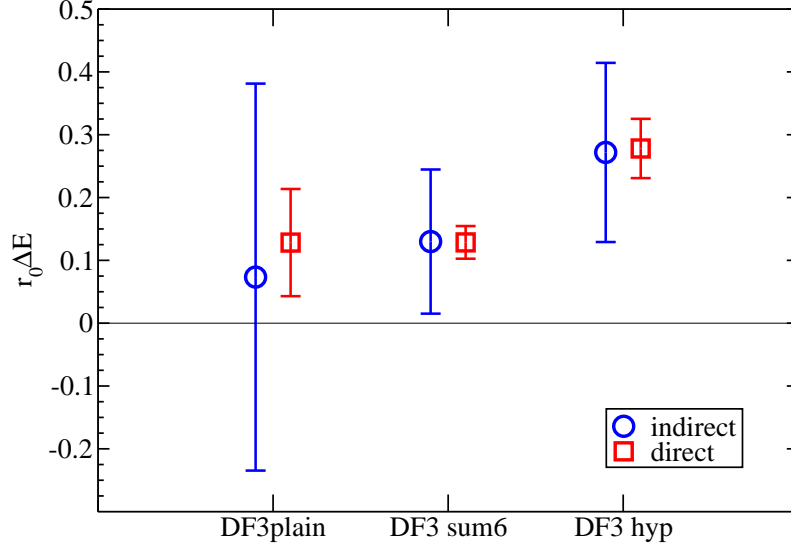


FIG. 28: (Color online) The Spin-Orbit splittings of D-wave states for the “DF3” lattice.

the $1P_+$ and $1P_-$ states in two different ways:

1. *Indirectly* by simply calculating the difference using the energies given by the fits in Eq. 2, when the P_+ and P_- data are fitted separately.
2. Combining the P_+ and P_- data and fitting the ratio $C_2(P_+)/C_2(P_-)$, which enables us to go *directly* for the spin-orbit splitting, $m_{1P_+} - m_{1P_-}$.

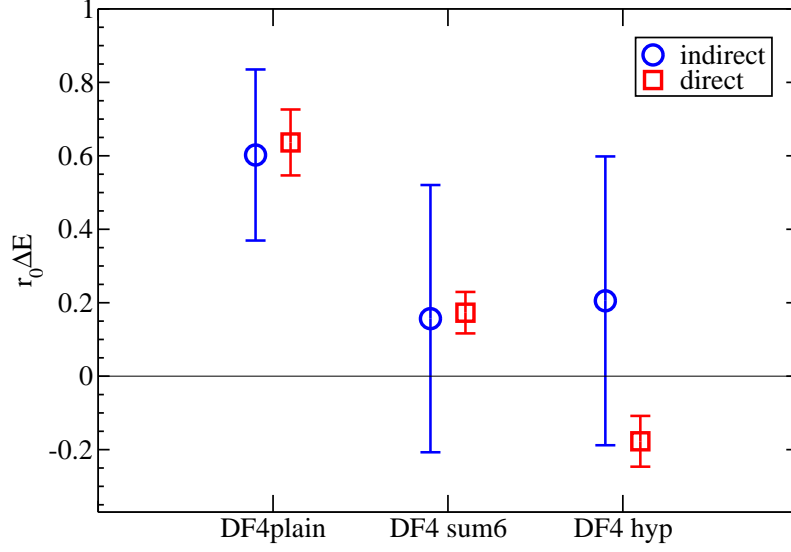


FIG. 29: (Color online) The Spin-Orbit splittings of D-wave states for the “DF4” lattice.

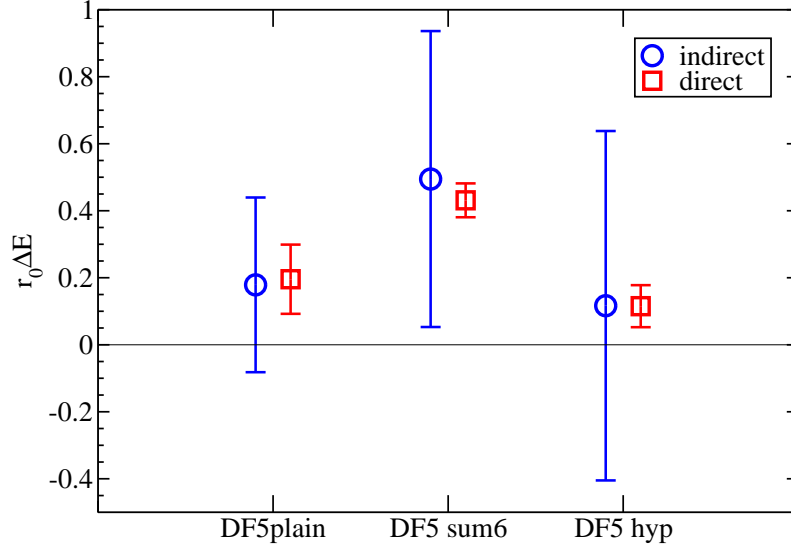


FIG. 30: (Color online) The Spin-Orbit splittings of D-wave states for the “DF5” lattice.

In the latter case, the expression (for a given fuzzing) is

$$\frac{C_2(P_+)}{C_2(P_-)} = A e^{-\Delta m_1 T} \left[\frac{1 + b_2^+ e^{-\Delta m_2^+ T} + b_3^+ e^{-\Delta m_3^+ T}}{1 + b_2^- e^{-\Delta m_2^- T} + b_3^- e^{-\Delta m_3^- T}} \right], \quad (8)$$

where

$$\begin{aligned}
\Delta m_1 &= m_{1P_+} - m_{1P_-} , \\
\Delta m_2^+ &= m_{2P_+} - m_{1P_+} , \\
\Delta m_2^- &= m_{2P_-} - m_{1P_-} , \\
\Delta m_3^+ &= m_{3P_+} - m_{1P_+} \text{ and} \\
\Delta m_3^- &= m_{3P_-} - m_{1P_-} .
\end{aligned}$$

We get the best results by fitting Δm_1 , Δm_2^+ , Δm_2^- and the coefficients A , b_2^+ and b_2^- , but fixing the remaining mass differences and b 's from the individual two-point correlator fits (equation 2 and Table II). Thus

$$b_3^+ = \frac{a_{3,f_1}(P_+)a_{3,f_2}(P_+)}{a_{1,f_1}(P_+)a_{1,f_2}(P_+)} \text{ and } b_3^- = \frac{a_{3,f_1}(P_-)a_{3,f_2}(P_-)}{a_{1,f_1}(P_-)a_{1,f_2}(P_-)} \quad (9)$$

for given values of fuzzing indices f_1 , f_2 . The D-wave spin-orbit splitting is also extracted in a similar manner. The results of the fits are given in Tables X, XI and in Figs. 25–30. In all cases the errors on the direct estimates are much smaller than those on the indirect ones. Also in most cases the direct and indirect estimates are consistent with each other — the only exception being the P-wave “sum6” estimates. There the direct value is somewhat lower than the indirect estimate. In fact this difference brings the “sum6” direct estimate closer to the “hyp” value, and lends support to the preferred “hyp” estimate, which in all three cases gives a small P-wave spin-orbit splitting (SOS), consistent with zero, for the “hyp” configurations. The D-wave spin-orbit splitting (SOS) results are more varied, but the “DF3hyp” lattice suggests clearly a positive, non-zero D-wave SOS. However, the “DF4hyp” and “DF5hyp” estimates are considerably smaller, becoming negative for the “DF4hyp”. At present it is not clear whether this is a lattice artefact due to, say, not being in the continuum limit, or that indeed the D-wave results are more dependent on m_q than in the P-wave case.

VI. A MODEL BASED ON THE DIRAC EQUATION

Since the mass of the heavy quark is infinite, we have for a potential description essentially a one-body problem. Therefore, a simple model based on the Dirac equation is used to try to describe the lattice data. The potential in the Dirac equation has the usual linearly rising

scalar part, $b_{\text{sc}}r$, but in addition a vector part $b_{\text{vec}}r$ is added. The one gluon exchange term, $a_{\text{OGE}} \cdot V_{\text{OGE}}$, where

$$V_{\text{OGE}} = -\frac{4}{3} \frac{\alpha_s(r)}{r}, \quad (10)$$

with the running coupling constant $\alpha_s(r)$ given by

$$\alpha_s(r) = \frac{2}{\pi} \int_0^\infty dk \frac{\sin(kr)}{k} \alpha_s(k^2) \quad (11)$$

and

$$\alpha_s(k^2) = \frac{12\pi}{27} \frac{1}{\ln[(k^2 + 4m_g^2)/(\Lambda_{\text{QCD}}^2)]}. \quad (12)$$

Here, guided by fits to various meson masses using the Blankenbecler–Sugar equation, we fix $\Lambda_{\text{QCD}} = 260$ MeV and the dynamical gluon mass $m_g = 290$ MeV (see [19] for details). The potential also has a scalar term $m\omega L(L+1)$, which seems to be needed to increase the energy of D-wave states. This type of term arises in flux tube models, where a flux tube’s rotational energy is proportional to $L(L+1)$ (like in Isgur–Paton flux tube model, [20]).

The lines in the energy spectrum plot (Fig. 31) show three Dirac model fits from Table XII with $m = 560$ MeV (the constituent quark mass, from [19]) and $a_{\text{OGE}} = 1.00$. Attempts to also vary a_{OGE} easily lead to instabilities. The solid line, labelled “fit 1”, is a fit to three “DF3hyp” energy differences: $1P_-$ and $1D_-$ with respect to the ground state, and the P-wave spin-orbit splitting (direct estimate) $\text{SOS}(1P)$ [i.e. $E(1P_+) - E(1P_-)$]. The fit to these energies is acceptable with total $\chi^2 = 1.68$, but as soon as a fourth state [e.g. $\text{SOS}(D)$] is added a good χ^2 can no longer be achieved. The dashed line, “fit 2”, shows an attempt to fit “DF3hyp” $1P_-$, $\text{SOS}(1P)$, $1D_-$ and $\text{SOS}(1D)$. The χ^2 is not good, and letting a_{OGE} vary does not help: that only leads to unphysical values for the parameters. Using a different constituent quark mass, say $m = 490$ MeV from [21], gives basically the same fits (the changes are minimal). “Fit 3” is a fit to “DF3sum6” $1P_-$, $\text{SOS}(1P)$, $1D_-$ and $\text{SOS}(1D)$, and is shown in the figure for comparison. The fits to “DF3sum6” energies are also shown in Table XII. In Fig. 32 the same Dirac model fits are shown for the excited states. Here it can be seen that the fit is about 500 MeV lower than the lattice results, and the shift seems to be constant for both lattices (“DF3sum6” and “DF3hyp”) for all states, except the 2S. There is no obvious reason why the Dirac model should underestimate the first radial excitations by a constant amount, but a term of the form $0.5(n-1)$ GeV could be included in the model to improve the fit to excited states and be interpreted as a flux tube effect in

Case	b_{sc} [GeV/fm]	b_{vec} [GeV/fm]	ω	total χ^2
sum6 P_- , SOS(1P)	1.168(2)	0.0	0.0	7.8
sum6 P_- , SOS(1P)	0.86(13)	0.57(18)	0.0	0.0
sum6 P_- , SOS(1P), D_-	0.372(14)	0.0	0.0916(14)	4.5
sum6 P_- , SOS(1P), D_- , SOS(1D)	0.265(4)	0.571(13)	0.0696(11)	2.1
hyp P_- , SOS(1P)	1.294(10)	0.0	0.0	0.54
hyp P_- , SOS(1P)	1.40(18)	-0.2(2)	0.0	0.00
hyp P_- , SOS(1P), D_-	0.763(9)	0.0	0.0554(9)	1.83
hyp P_- , SOS(1P), D_- , SOS(1D)	0.48(5)	0.26(2)	0.066(5)	34.3

TABLE XII: Dirac model fits for “DF3”. Here $a_{\text{OGE}} = 1$ and constituent quark mass $m = 560$ MeV. Fits are attempted for “DF3sum6” and “DF3hyp”. A “perfect” fit (2 fit parameters, 2 data points) can be found for P_- and the P-wave spin-orbit splitting, if both scalar and vector linear potentials are used. However, all P- and D-wave data [P_- , SOS(1P), D_- , SOS(1D)] can not be fitted using the two linear rising potentials and adding a scalar term $m\omega L(L+1)$ still does not give a good χ^2 .

the same philosophy as the $\omega L(L+1)$ term. However, as the fit to the ground state energies is poor, this improvement is not pursued.

VII. CONCLUSIONS

- With the “DF3hyp” lattice, our predictions for the 1^+ and 2^+ P-wave state masses agree very well with the experimental results. We also predict that the masses of the two lower P-wave states (0^+ and 1^+) should lie only a few MeV below the BK and B^*K thresholds respectively.
- Also with the “DF3hyp” lattice, the P-wave spin-orbit splitting is small (essentially zero), but the D-wave spin-orbit splitting is clearly non-zero and positive. In contrast, another lattice group finds the P-wave spin-orbit splitting to be positive (about 35 MeV) and the D-wave SOS to be slightly negative (see [15]), i.e. they seem to observe the famous inversion [21]. However, the recent European Twisted Mass Collaboration results find the P-wave SOS to be negative and the D-wave SOS to be small [9]. One clearly needs to go to the continuum limit before any definite conclusions can

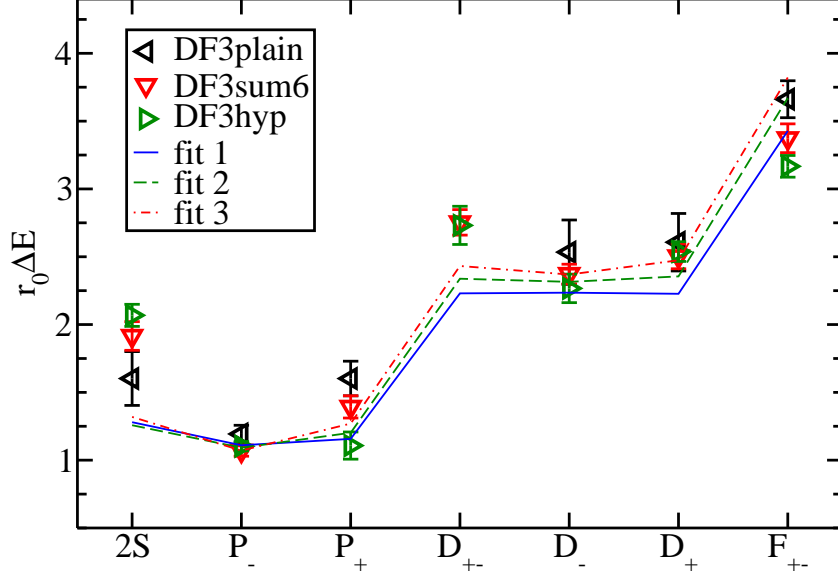


FIG. 31: (Color online) Energy spectrum of the heavy-light meson and three Dirac model fits. “Fit 1” is a fit to “DF3hyp” $1P_-$, $\text{SOS}(1P)$ and $1D_-$, whereas “fit 2” is an attempt to fit “DF3hyp” $1P_-$, $\text{SOS}(1P)$, $1D_-$ and $\text{SOS}(1D)$ (see Table XII). “Fit 3” is a fit to “DF3sum6” $1P_-$, $\text{SOS}(1P)$, $1D_-$ and $\text{SOS}(1D)$, and is shown here for comparison.

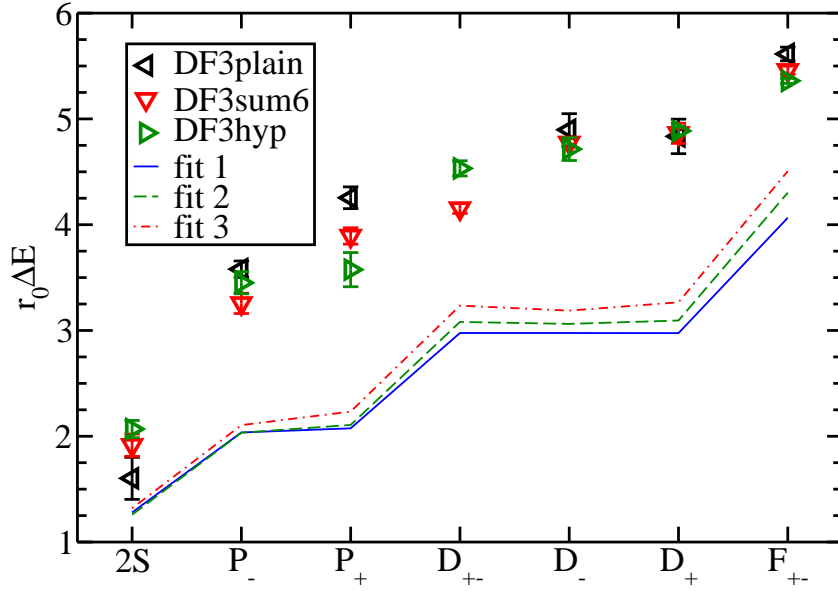


FIG. 32: (Color online) Energies of the first radial excitations of the heavy-light meson and the same Dirac model fits shown in Fig. 31.

be made.

In [14] Woo Lee and Lee suggest that the absence of spin-orbit inversions can be explained by chiral radiative corrections in the potential model. Small spin-orbit splittings throughout the meson spectrum could be explained by a relativistic symmetry in the Dirac Hamiltonian discussed in [22]. This would indicate that the scalar potential is (at least approximately) equal to the vector potential.

- The one-body Dirac equation model with one-gluon exchange, vector and scalar linear potentials and a scalar term $m\omega L(L+1)$ (like a flux tube rotational energy) is not good enough to describe the entire lattice energy spectrum. Therefore, one should be very careful in using such simple potentials to describe the interaction between quarks.

Acknowledgements

I am grateful to my collaborators, Professors A.M. Green and C. Michael, and to the UKQCD Collaboration for providing the lattice configurations. I wish to thank Professor Philippe de Forcrand for useful comments and also the Center for Scientific Computing in Espoo, Finland, for making available the computer resources. This work was supported in part by the EU Contract No. MRTN-CT-2006-035482, “FLAVIANet”.

APPENDIX A: SOME CHECKS

To check that the different results for different smearings (specifically for the spin-orbit splittings) are a real effect and not due to some biasing element in the final analysis, we plot the basic signals in Figs. 33 for the P-wave. The signals clearly are different for “DF3sum6” and “DF3hyp”, supporting the results of the complete analysis in Fig. 25.

-
- [1] C. R. Allton *et al.* (UKQCD Collaboration), Phys. Rev. D 65, 054502 (2002); C. R. Allton, A. Hart, D. Hepburn, A. C. Irving, B. Joó, C. McNeile, C. Michael and S. V. Wright (UKQCD Collaboration), Phys. Rev. D 70, 014501 (2004)

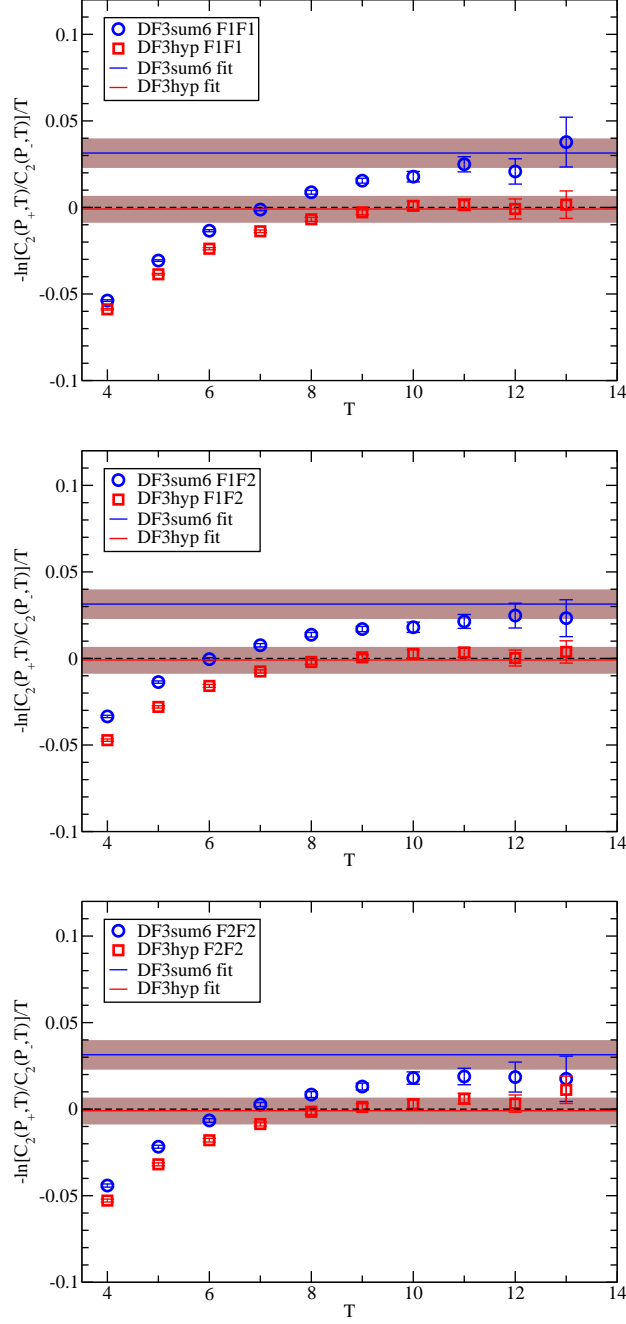


FIG. 33: (Color online) To study the observed difference in the P-wave spin-orbit splitting between the “DF3hyp” and “DF3sum6” configurations seen in Fig. 25, these figures show the logarithm of the ratio $C_2(P_+, T)/C_2(P_-, T)$ divided by T for “DF3hyp” and “DF3sum6” for the three possible fuzzing combinations (from top to bottom: F1F1, F1F2 and F2F2). This should exhibit a plateau for large enough T . The horizontal lines show the fit results from the full analysis (F1F1, F1F2 and F2F2 all included). The shaded area shows the estimated errors.

- [2] UKQCD Collaboration, A. M. Green, J. Koponen, C. Michael, C. McNeile and G. Thompson, Phys. Rev. D 69, 094505 (2004), and UKQCD Collaboration, J. Koponen, [hep-lat/0411015](#)
- [3] UKQCD Collaboration, P. Lacey, C. Michael, P. Boyle and P. Rowland, Phys. Rev. D 54, 6997 (1996)
- [4] UKQCD Collaboration, C. Michael and J. Peisa, Phys. Rev. D 58, 034506 (1998)
- [5] A. Hasenfratz and F. Knechtli, Phys. Rev. D 64, 034504 (2001)
- [6] M. Della Morte, A. Shindler and R. Sommer, JHEP 0508, 051 (2005)
- [7] UKQCD Collaboration, A. M. Green, J. Ignatius, M. Jahma, J. Koponen, C. McNeile and C. Michael, PoS LAT2005 (2005) 205, and UKQCD Collaboration, J. Koponen, PoS LAT2006 (2006) 112
- [8] UKQCD Collaboration, J. Koponen, Nucl. Phys. Proc. Suppl. 140, 437 (2005) and [hep-lat/0411015](#). Part of the work is in progress.
- [9] K. Jansen, C. Michael, A. Shindler and M. Wagner, [arXiv:0808.2121 \[hep-lat\]](#)
- [10] T. Burch, D. Chakrabarti, C. Hagen, C. B. Lang, M. Limmer, T. Maurer and A. Schäfer, PoS LAT2007 (2007) 91
- [11] W.-M. Yao *et al.*, J. Phys. G 33, 1 (2006)
- [12] CDF and DØ Collaborations, R. K. Mommensen, Nucl. Phys. Proc. Suppl. **170**, 172 (2007); CDF Collaboration, T. Aaltonen *et al.*, Phys. Rev. Lett. **100**, 082001 (2008); DØ Collaboration, V. M. Abazov *et al.*, Phys. Rev. Lett. **100**, 082002 (2008)
- [13] V. Poireau, [arXiv:0705.3716 \[hep-ex\]](#), published in “Munich 2007, Deep-inelastic scattering”, pp. 857-860
- [14] I. Woo Lee and T. Lee, Phys. Rev. D 76, 014017 (2007)
- [15] J. Foley, A. Ó Cais, M. Peardon and S. Ryan, PoS LAT2006 (2006) 196 and Phys. Rev. D 75, 094503 (2007)
- [16] BABAR Collaboration, B. Aubert, Phys. Rev. Lett. 97, 222001 (2006)
- [17] Belle Collaboration, K. Abe *et al.*, [arXiv:hep-ex/0608031](#), presented at the 33rd International Conference on High Energy Physics (ICHEP 06), Moscow
- [18] P. Colangelo, F. De Fazio and S. Nicotri, Phys. Lett. B 642, 48 (2006)
- [19] T. A. Lähde, C. Nyfält and D. O. Riska, Nucl. Phys. A674, 141 (2000)
- [20] N. Isgur and J. Paton, Phys. Rev. D 31, 2910 (1985)
- [21] H. J. Schnitzer, Phys. Rev. D 18, 3482 (1978) and Phys. Lett. B 226, 171 (1989)

[22] P. R. Page, T. Goldman and J. N. Ginocchio, Phys. Rev. Lett. 86, 204 (2001)